Kv3.3 subunits control presynaptic action potential waveform and neurotransmitter release at a central excitatory synapse

Amy Richardson[1†], Victoria Ciampani[1], Mihai Stancu[2], Kseniia Bondarenko[1‡], Sherylanne Newton[1§], Joern R Steinert[1#], Nadia Pilati[3], Bruce P Graham[4], Conny Kopp-Scheinpflug[2], Ian D Forsythe[1*]

[1]Auditory Neurophysiology Laboratory, Department of Neuroscience, Psychology and Behaviour, College of Life Sciences, University of Leicester, Leicester, United Kingdom; [2]Division of Neurobiology, Faculty of Biology, Ludwig-Maximilians-University, Munich, Germany; [3]Autifony S.r.l., Istituto di Ricerca Pediatrica Citta'della Speranza, Corso Stati Uniti, Padova, Italy; [4]Computing Science and Mathematics, Faculty of Natural Sciences, University of Stirling, Stirling, United Kingdom

*For correspondence:
idf@le.ac.uk

Present address: †Department of Clinical and Experimental Epilepsy, Institute of Neurology, University College London, London, United Kingdom; ‡Institute of Immunology and Infection Research, University of Edinburgh, Edinburgh, United Kingdom; §UCL Ear Institute, University College London, London, United Kingdom; #School of Life Sciences, Medical School, University of Nottingham, Nottingham, United Kingdom

Summary: Kv3 potassium currents mediate rapid repolarisation of action potentials (APs), supporting fast spikes and high repetition rates. Of the four Kv3 gene family members, Kv3.1 and Kv3.3 are highly expressed in the auditory brainstem and we exploited this to test for subunit-specific roles at the calyx of Held presynaptic terminal in the mouse. Deletion of Kv3.3 (but not Kv3.1) reduced presynaptic Kv3 channel immunolabelling, increased presynaptic AP duration and facilitated excitatory transmitter release; which in turn enhanced short-term depression during high-frequency transmission. The response to sound was delayed in the Kv3.3KO, with higher spontaneous and lower evoked firing, thereby reducing signal-to-noise ratio. Computational modelling showed that the enhanced EPSC and short-term depression in the Kv3.3KO reflected increased vesicle release probability and accelerated activity-dependent vesicle replenishment. We conclude that Kv3.3 mediates fast repolarisation for short precise APs, conserving transmission during sustained high-frequency activity at this glutamatergic excitatory synapse.

Editor's evaluation

This work shows that Kv3.3 potassium channels play a major role in shaping the presynaptic action potential waveform of calyx-type auditory synapses. Mice that lack Kv3.3 showed auditory response deficits, including increases of spike latency and jitter. Overall, the study shows the uniquely important role for Kv3.3 channels in the fast synaptic transmission between the neurons that compute sound localization in mammals.

Introduction

Kv3 voltage-gated potassium currents rapidly repolarise APs and underlie fast-spiking neuronal phenotypes, enabling high-frequency firing with temporal precision (*Rudy and McBain, 2001*; *Kaczmarek and Zhang, 2017*). Kv3 channels are expressed throughout the brain including the hippocampus, cortex, cerebellum, and auditory brainstem (*Weiser et al., 1994*; *Du et al., 2000*; *Lien and Jonas, 2003*). They influence dendritic integration (*Zagha et al., 2010*) and somatic AP waveform (*Espinosa et al., 2008*; *Rowan et al., 2014*; *Choudhury et al., 2020*), but Kv3 channels are also located in

particular axons, including nodes of Ranvier (*Devaux et al., 2003*) and synaptic terminals (*Schneggenburger and Forsythe, 2006*).

There are four Kv3 genes (*kcnc1-4*) specifying alpha subunits (Kv3.1–3.4) that assemble as tetramers (*Coetzee et al., 1999*; *Rudy et al., 1999*). The transmembrane domains are generally well conserved across subunits, but both the N- and C-terminal domains have diverse sequences, creating distinct inactivation kinetics, interaction with cytoskeletal proteins (*Blosa et al., 2015*; *Stevens et al., 2021*) and regulation by phosphorylation (*Macica et al., 2003*; *Song et al., 2005*; *Desai et al., 2008*). Kv3 channels display ultra-fast kinetics (*Grissmer et al., 1994*; *Labro et al., 2015*) with half-activation at positive voltages, making them particularly effective in AP repolarisation (*Brew and Forsythe, 1995*). N-type inactivation is a powerful means of regulating K$^+$ channel activity (*Hoshi et al., 1990*) and inactivation in the Kv3 family is influenced by the subunit(s) expressed and their regulation by protein phosphorylation (see *Kaczmarek and Zhang, 2017*).

Transgenic knockouts of one subunit generally show mild phenotypes, consistent with heterogeneous composition of native channels and functional redundancy (*Joho et al., 1999*; *Espinosa et al., 2001*; *Joho et al., 2006*). Co-expression of Kv3.1 and Kv3.3 has been widely observed in different brain regions (*Chang et al., 2007*) and we recently showed that principal neurons of the medial nucleus of the trapezoid body (MNTB) within the auditory brainstem, have Kv3 channels composed of Kv3.1 and Kv3.3 subunits. In the MNTB, in contrast to the lateral superior olive, each subunit type can compensate for deletion of the other (*Choudhury et al., 2020*).

Changes in AP waveform at the synaptic terminal critically control calcium influx and neurotransmitter release (*Borst and Sakmann, 1998*; *Forsythe et al., 1998*; *Yang et al., 2014*), this in turn influences short-term plasticity (*Sakaba and Neher, 2003*; *Hennig et al., 2008*; *Neher and Sakaba, 2008*; *Neher, 2017*; *Lipstein et al., 2021*) and presynaptic forms of long term potentiation at mossy fiber terminals (*Geiger and Jonas, 2000*). Indeed, tuning of voltage-gated sodium and potassium channel kinetics not only enhances fast signaling, but also increases metabolic efficiency (*Hu et al., 2018*). In the present study, we took advantage of the calyx of Held giant synapse in the MNTB to investigate the role of Kv3 subunits at that presynaptic terminal. These binaural auditory nuclei must rapidly integrate AP trains transmitted from left and right cochlea with microsecond accuracy (*Beiderbeck et al., 2018*; *Joris and Trussell, 2018*; *Karcz et al., 2011*). The region expresses Kv3.1 and Kv3.3 subunits, with little or no Kv3.2 and Kv3.4 (*Choudhury et al., 2020*). This synapse is optimised for speed and fidelity (*Taschenberger et al., 2002*) and is operating at the 'biophysical limit' of information processing, in that fast conducting axons and giant synapses with nano-domain localisation of P/Q Ca^{2+} channels, combine with postsynaptic expression of fast AMPARs, short postsynaptic membrane time-constants and exceptionally rapid APs to enable binaural sound localisation (*Schneggenburger and Forsythe, 2006*; *Neher and Sakaba, 2008*; *Joris and Trussell, 2018*; *Young and Veeraraghavan, 2021*).

In this study, we test whether Kv3.1 or Kv3.3 subunits have a specific presynaptic role by examining the calyx of Held AP waveform and transmitter release on deletion of either subunit. We show that Kv3.3 subunits are localised to the presynaptic terminal and that their deletion increases transmitter release. We demonstrate the role of Kv3.3 in enhancing the speed and reliability of brainstem binaural auditory processing and conclude that presynaptic Kv3.3 subunits are essential for fast AP repolarisation at this excitatory synapse.

Results

The experiments reported here were conducted using CBA/CrL wildtype mice or transgenic mice backcrossed onto CBA/CrL that lacked either Kv3.3 or Kv3.1 (the genotypes are referred to as WT, Kv3.3KO and Kv3.1KO). We previously reported that Kv3.1 and Kv3.3 mRNAs are highly expressed in the MNTB, and no compensation for either subunit in the respective knockouts was observed (*Choudhury et al., 2020*). The influence of these deletions was assessed in vivo using extracellular recording from the MNTB and in vitro using whole cell patch clamp from the calyx of Held and MNTB principal neurons. Additionally, immunohistochemical localisation of Kv3.1 and Kv3.3 was determined using expansion microscopy. Together, these methods were applied to determine the contribution of Kv3 subunits to the presynaptic AP waveform, to assess the impact on transmitter release and determine how this impacts the response to sound. As an additional control, we confirmed that both Kv3.1 and Kv3.3 mRNA are present in the cochlear nucleus where globular bushy cells give rise to the calyx of Held synaptic terminal. The percent contribution of each subunit gene to the cochlear

nucleus Kv3 mRNA was 30.3% ± 9.1% (Kv3.1), 7.7% ± 2.8% (Kv3.2), 52.0% ± 6.0% (Kv3.3), and 10.0% ± 1.6% (Kv3.4; for data see *Figure 1—figure supplement 1* and summary statistics). These values are similar to those measured in the MNTB (*Choudhury et al., 2020*). Additionally, immunohistochemistry confirmed that both spiral ganglion neurons and cochlear nucleus have broad neuronal staining for Kv3.1 and Kv3.3 and as validated using tissue from knockout mice (*Figure 1—figure supplements 2 and 3*).
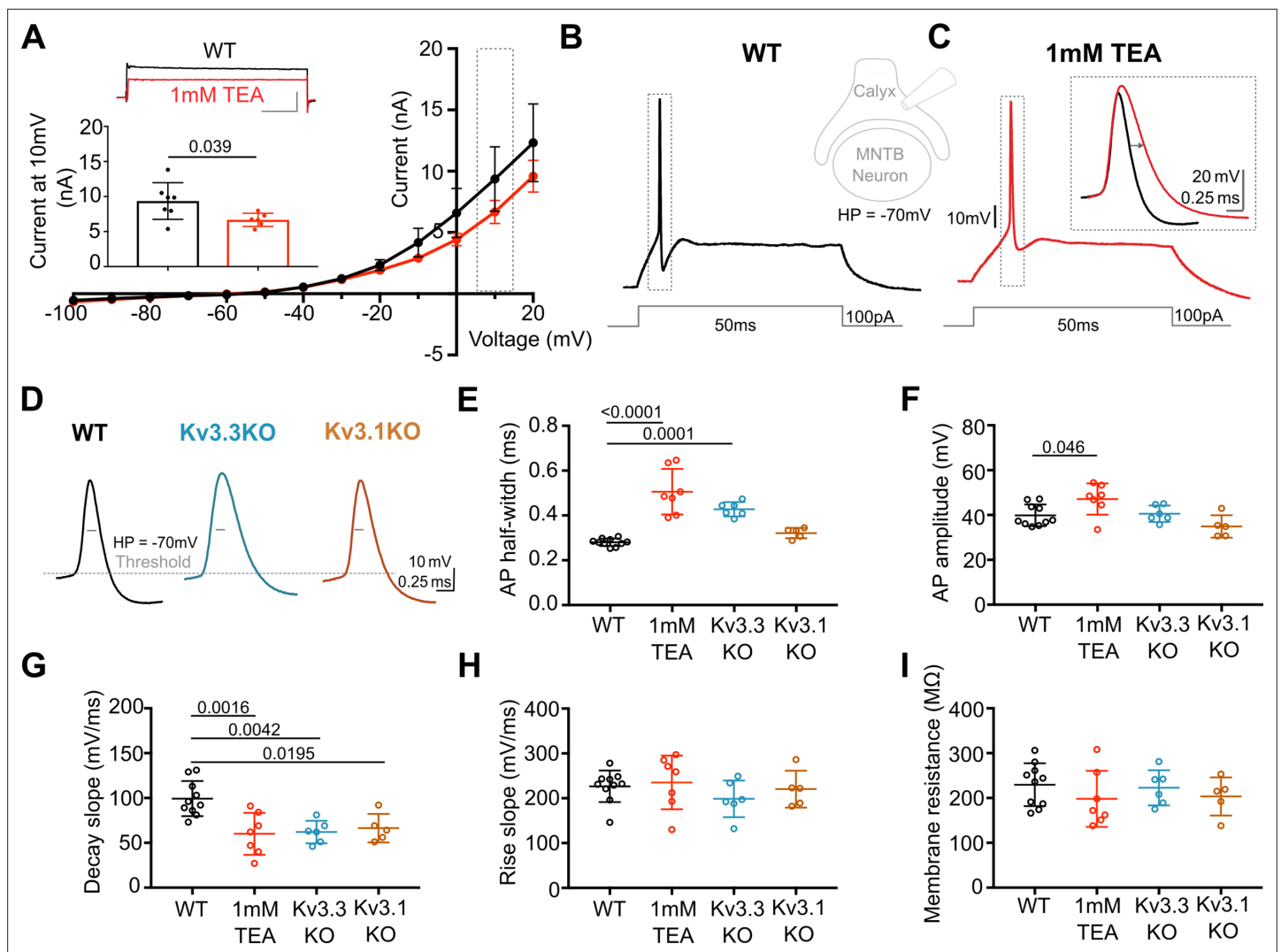
Kv3 channels contribute to action potential repolarisation at the calyx of Held terminal

Previous reports have employed potassium channel blockers (4-aminopyridine or tetraethylammonium) to show that Kv3 currents contribute to fast repolarisation of APs in the MNTB (*Forsythe, 1994*; *Brew and Forsythe, 1995*; *Wang et al., 1998*). Low concentrations of extracellular TEA (1 mM) give a relatively selective block of Kv3 potassium channels (*Johnston et al., 2010*). Whole terminal voltage-clamp recordings of the calyx terminal revealed an outward current, as shown in the current-voltage relations in *Figure 1A*, with 1 mM TEA blocking 28.7% of the total outward current at a command voltage of +10 mV (current amplitude in WT = 9.37 ± 2.6 nA, n=7 calyces; WT+TEA = 6.68±0.9 nA, n=6; unpaired t-test, p=0.037; mean ± SD). Injection of depolarising current steps (100 pA, 50ms) under current-clamp triggered a single AP in the presynaptic terminal, (*Figure 1B*) which increased in duration on perfusion of 1 mM TEA (*Figure 1C*; with inset showing ±TEA overlay). In tissue from WT mice the mean AP half-width increased from 0.28±0.02ms (control; n=9) to 0.51±0.1ms (n=7) in the presence of 1 mM TEA (*Figure 1E*), supporting the hypothesis that presynaptic Kv3 channels are present and contribute to AP repolarisation at the calyx of Held.

AP duration increased in terminals from Kv3.3KO mice, similar to that from WT mice in the presence of TEA. In contrast, the AP duration recorded from terminals of Kv3.1KOs was comparable to WT APs (see *Figure 1D and E*). AP half-widths increased from 0.28±0.02ms in WT (n=9) and 0.32±0.02ms Kv3.1KOs (n=5) to 0.43±0.03ms in Kv3.3KO mice (n=6) and 0.51±0.1ms in WT+TEA (n=7). This increase in duration at 50% amplitude was accompanied by a slowed rate of AP decay in both Kv3.3KO terminals and WT terminals upon perfusion of TEA (*Figure 1G*, one-way ANOVA, Tukey's post hoc, Kv3.3KO vs WT p=0.0042; TEA vs WT p=0.0016) with no changes in the rising phase of the AP (one-way ANOVA, p=0.50; *Figure 1H*), nor in the resting (input) membrane conductance (one-way ANOVA, p=0.56; *Figure 1I*) or AP threshold (one-way ANOVA, p=0.96; see statistics table). Similar significant changes in AP duration were observed at 25% and 75% amplitudes for deletion of Kv3.3, but deletion of Kv3.1 did not significantly change AP duration at 25%, 50%, or 75% amplitude (see *Figure 1—figure supplement 4*). This suggests that Kv3.3 subunits are of most importance for presynaptic Kv3 channels and fast AP repolarisation . Despite the lack of a significant increase in action potential duration measured in Kv3.1KOs, the rate of decay was significantly slowed from 99±20 mV/ms (n=10) to 66±16 mV/ms (n=5; one-way ANOVA, Tukey's post hoc, p=0.02), consistent with Kv3.1 having a secondary role in presynaptic AP repolarisation, as might be expected from their localisation at axonal nodes of Ranvier (*Devaux et al., 2003*) and potential to form heteromers with Kv3.3 subunits.

Immunohistochemical localisation shows that presynaptic Kv3 channels require the presence of a Kv3.3 subunit

Since Kv3 channels are present in both the presynaptic calyx of Held and the postsynaptic MNTB neuron, conventional fluorescence immunohistochemistry fails to resolve any differential localisation of particular subunits in the presynaptic or postsynaptic membranes. An additional complication is that few studies have localised both Kv3.1 and Kv3.3 subunits, most focus on imaging one subunit (usually Kv3.1). Electron microscopic studies demonstrated that Kv3.1b is present in the membrane of the non-release face of the calyx of Held (*Elezgarai et al., 2003*), while *Wu et al., 2021* show that Kv3.3 is present at the release face of the calyx. Kv3.3 has also been demonstrated at terminals in the medial vestibular nucleus (*Brooke et al., 2010*) at the neuromuscular junction (*Brooke et al., 2004*) and in hippocampal mossy fibers (*Chang et al., 2007*). Hence, there is histological evidence for Kv3.1 and Kv3.3 at specific presynaptic terminals, but they are not universally expressed at all synaptic terminals.

Figure 1. Presynaptic AP duration is increased by TEA or Kv3.3 deletion. (**A**) Current-Voltage (I–V) relationship for potassium currents in the calyx of Held terminal of WT mice (P10–P12) in control (black; n=7 terminals, 4 mice) and TEA, 1 mM (red, n=6 terminals, 5 mice; HP = –70 mV). **Inset (top):** Example current traces in response to voltage command of +10 mV step (grey box in IV) in WT (black) and WT +1 mM TEA (red). Scale bars = 5 nA and 20ms. **Inset (lower):** Bar graph of mean currents ± SD, measured on step depolarisation to +10 mV (from HP –70 mV) ±1 mM TEA. Outward Currents are significantly reduced by TEA (student's t-test, unpaired, P=0.0386). (**B**) WT calyx AP (black trace) evoked by 100 pA step current injection; **inset** - diagram of recording configuration. (**C**) WT calyx AP in the presence of TEA (1 mM, red trace); inset – overlaid WT APs ±TEA (red) as indicated by dotted box (grey) around APs in B and C. (**D**) Representative AP traces from calyx terminals of WT (black), Kv3.3KO (blue), and Kv3.1KO (orange); double arrows indicate the half-width of WT AP. AP threshold is indicated by the grey dashed line. (**E**) AP half-width measured as time difference between rise and decay phases at 50% maximal amplitude. Half-width is significantly increased in TEA and in Kv3.3KO; N is individual terminals: WT N=9 from 6 animals; TEA = 7 from 5 mice; Kv3.3KO = 6 from 3 mice and Kv3.1KO = 5 from 3 mice. (**F**) AP amplitude, (**G**) AP Decay slope, (**H**) AP rise slope (10–90%) and (**I**) membrane resistance for calyceal recordings. Average data presented as mean ± SD. Statistical test (parts E-I) were one-way ANOVAs and Tukey's post hoc for multiple comparisons, with significant Ps indicated on the graph.

The online version of this article includes the following source data and figure supplement(s) for figure 1:

Source data 1. Relates to *Figure 1*.

Figure supplement 1. WT mRNA Levels for *Kcnc* family genes in the cochlear nucleus which show a similar pattern of expression to those measured previously for the MNTB (*Choudhury et al., 2020*).

Figure supplement 1—source data 1. Relates to *Figure 1—figure supplement 1*.

Figure supplement 2. Kv3.1 and Kv3.3 immunoreactivity in the cochlear nucleus of CBA WT mice.

Figure supplement 3. Kv3.1 and Kv3.3 are present in spiral ganglion neurons of CBA WT mice.

Figure 1 continued on next page

Figure 1 continued

Figure supplement 4. Repolarisation of the presynaptic AP is slowed during the entire length of the downstroke in the presence of 1 mM TEA and in Kv3.3KOs.

Figure supplement 4—source data 1. Relates to *Figure 1—figure supplement 4*.

Capitalising on using KO-validated antibodies (*Choudhury et al., 2020 Figure 1—figure supplement 3*), we have employed protein-retention expansion microscopy (*Asano et al., 2018*) to increase resolution and gain more precision in localising Kv3.1 and Kv3.3 subunits at the calyx of Held synaptic terminal. The technique employs a hydrogel to expand the tissue by ~4.5 x prior to confocal imaging. We compared the location of Kv3 subunits in the three genotypes: antibodies targeting Kv3.3 were employed in the Kv3.1KO, antibodies against Kv3.1 were used in tissues from the Kv3.3KO and both Kv3.1 and Kv3.3 antibodies were employed in WT tissue. This experiment asks whether either Kv3.1 or Kv3.3 subunits are necessary and sufficient to enable presynaptic localisation of Kv3 channels. Synaptic release sites were identified using bassoon antibodies (*Chen et al., 2013*) to label the presynaptic specialisation and the results are shown in *Figure 2*.

In *Figure 2*, the two quadrants on the left show Kv3.3 staining (in the Kv3.1KO above, and WT, below) and the two right quadrants show Kv3.1 staining (in the Kv3.3KO above, and WT, below) in yellow. All sections are co-stained with bassoon (purple). Each quadrant shows single optical sections from three different MNTB neuron/calyx pairs shown at lower magnification in the respective top row. Kv3.3 staining was clearly present in the presynaptic terminal profiles surrounding each of the 3 MNTB neurons which lacked Kv3.1 (*Figure 2A1–C1*). In contrast, Kv3.1 labelling (from the Kv3.3KO tissue) showed little evidence of presynaptic labelling (*Figure 2D1–F1*). As a positive control, Kv3.1 labelling was robust in the postsynaptic membrane; and indeed Kv3.3 is also clearly present in the postsynaptic membrane. Each neuron in rows 1 and 4 has two synaptic profiles indicated by the orange and green arrowheads, each of these synapses are shown enlarged below their neuron of origin in rows 2 and 3 and rows 5 and 6, respectively. Similar labelling profiles are observed in the WT tissue (lower quadrants of *Figure 2A4–F4*). As for the KO tissue, two examples of WT presynaptic profiles are indicated by the coloured arrows and their enlargement shown below each principal neuron. The Kv3.3 antibody staining was clearly observed in the presynaptic membrane on the non-release face of the WT synapse (for example see *Figure 2B2 and C3, A6*) and in some image sections the release face of the synapse, between bassoon labelling (see *Figure 2C3, B5 and A6*) was clear. It was hard to visualise presynaptic membrane staining with the Kv3.1 antibody in the Kv3.3KO tissue (*Figure 2D2, E3 and F2*); but some Kv3.1-stained membrane profiles were observed on the non-release face in the WT tissue (*Figure 2E5, E6 and F6*).

While the calyceal Kv3.3 staining in the WT is similar to that in the Kv3.1KO, the levels of Kv3.1 staining in the WT are higher (than in the Kv3.3KO) consistent with the hypothesis that Kv3.1 may gain access to the presynaptic compartment through heteromeric assembly with Kv3.3 subunits. This data shows that while both Kv3.1 and Kv3.3 subunits are present in the postsynaptic soma membrane, only Kv3.3 subunits are required to achieve trafficking of Kv3 channels to the presynaptic terminal; and there is some evidence that the presence of Kv3.3 permits access of Kv3.1 subunits to the terminal, while both Kv3.1 and Kv3.3 were localised to the postsynaptic plasma membrane in the WT tissue.

Deletion of Kv3.3 subunits increases calyceal-evoked EPSC amplitude

Transmitter release crucially depends on depolarisation of the presynaptic membrane and consequent calcium influx. Since Kv3 channels are present and involved in calyceal AP repolarisation, we assessed the physiological impact of each Kv3 subunit on transmitter release, and compared this to WT and to transmitter release following pharmacological block of presynaptic Kv3 channels using 1 mM TEA.

Whole cell patch recordings under voltage-clamp (HP = –40 mV, to inactivate voltage-gated Na$^+$ channels) were made from MNTB neurons possessing an intact calyx, in tissue from mice of each genotype and in the presence of 1 mM TEA. This allows comparison of the EPSC amplitude in four conditions: where Kv3 channels are intact (WT) and where they lack Kv3.1 or Kv3.3, and finally with all presynaptic Kv3 channels blocked (TEA). Unitary calyceal EPSCs were evoked in MNTB principal neurons as shown in *Figure 3A and F*. The global average for each condition and the unitary mean evoked EPSCs are overlaid from each genotype in *Figure 3F*. The dashed grey line shows the WT mean amplitude for comparison. The calyceal EPSCs recorded from Kv3.3KO mice were of larger peak
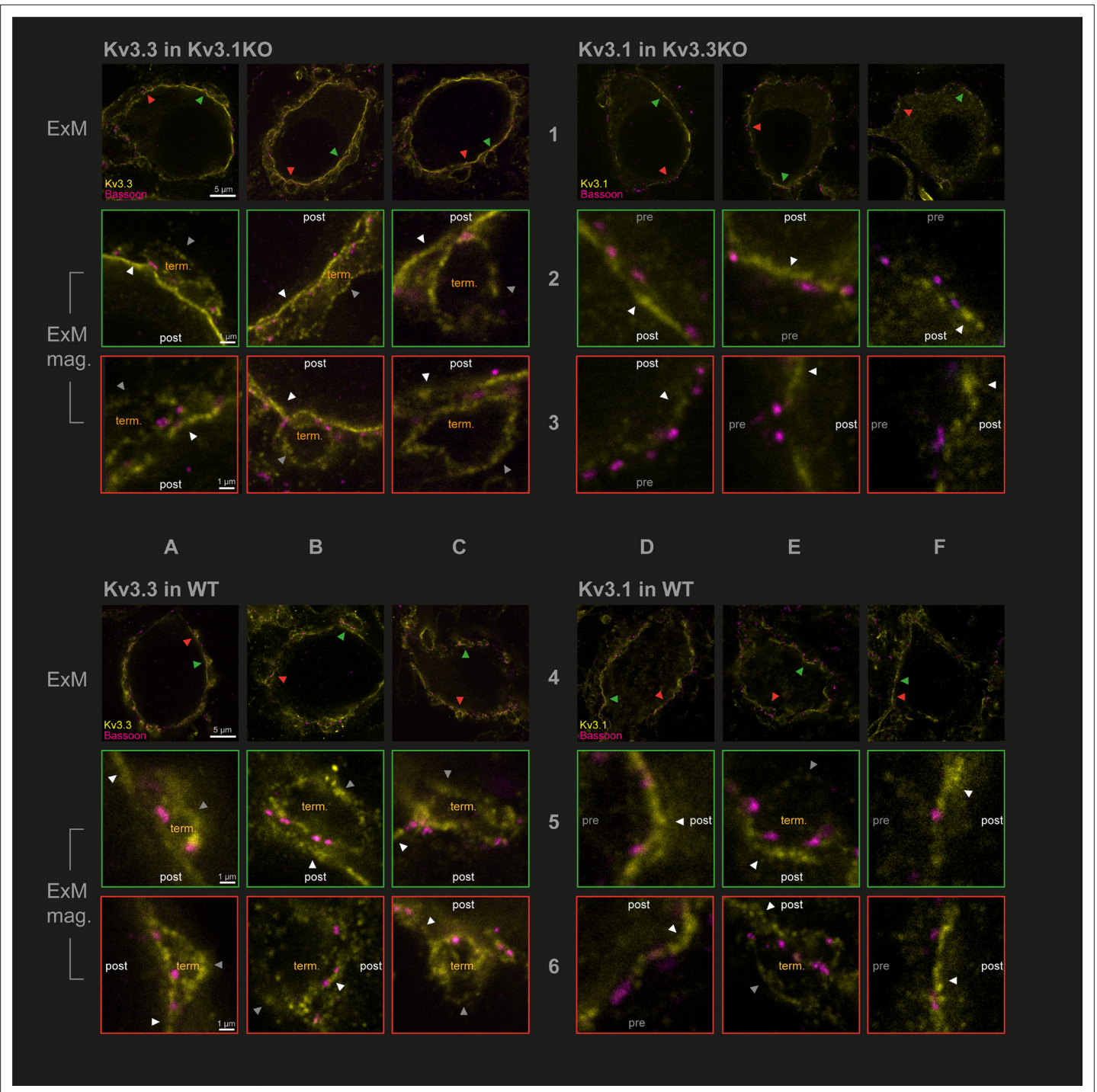
Figure 2. Protein-retention Expansion Microscopy (proExM) with confocal fluorescence imaging shows that Kv3.3 subunits are present in calyx of Held presynaptic terminal membrane. Individual images are identified in rows 1–6 and columns A-F, as indicated by the central labels. Four quadrants of 9 images are shown, each 3 × 3 matrix is from the named genotype and stained as specified in the title of each quadrant. The top row of each quadrant (rows 1 and 4) are single optical sections from 3 different MNTB neurons, in which their calyceal synaptic profiles are labelled with bassoon (purple) and co-labelled with either Kv3.1 or Kv3.3 antibodies (yellow): from Kv3.1KO and stained for Kv3.3 (**A1-C1**); the Kv3.3KO stained for Kv3.1 (**D1-F1**); WT stained for Kv3.3 (**A4-C4**); WT stained for Kv3.1 (**D4-F4**). In each MNTB neuron (rows 1 & 4) two synaptic regions of interest (ROI) containing bassoon are indicated by the red and green arrowheads. These magnified ROIs are displayed below (in rows 2+3 or 5+6) bordered by the same colour, respectively. The neuronal compartments are labelled: 'post' – postsynaptic; 'pre' – presynaptic; 'term' – synaptic terminal. In each image, the dark grey arrows point to presynaptic Kv3 labelling, and the white arrows point to postsynaptic Kv3 labelling. Scale bars are indicated for each row in column A (5 μm in rows 1 and 4: 1 μm in rows 2,3,5, and 6). Tissue was used from mice aged P28-P30.
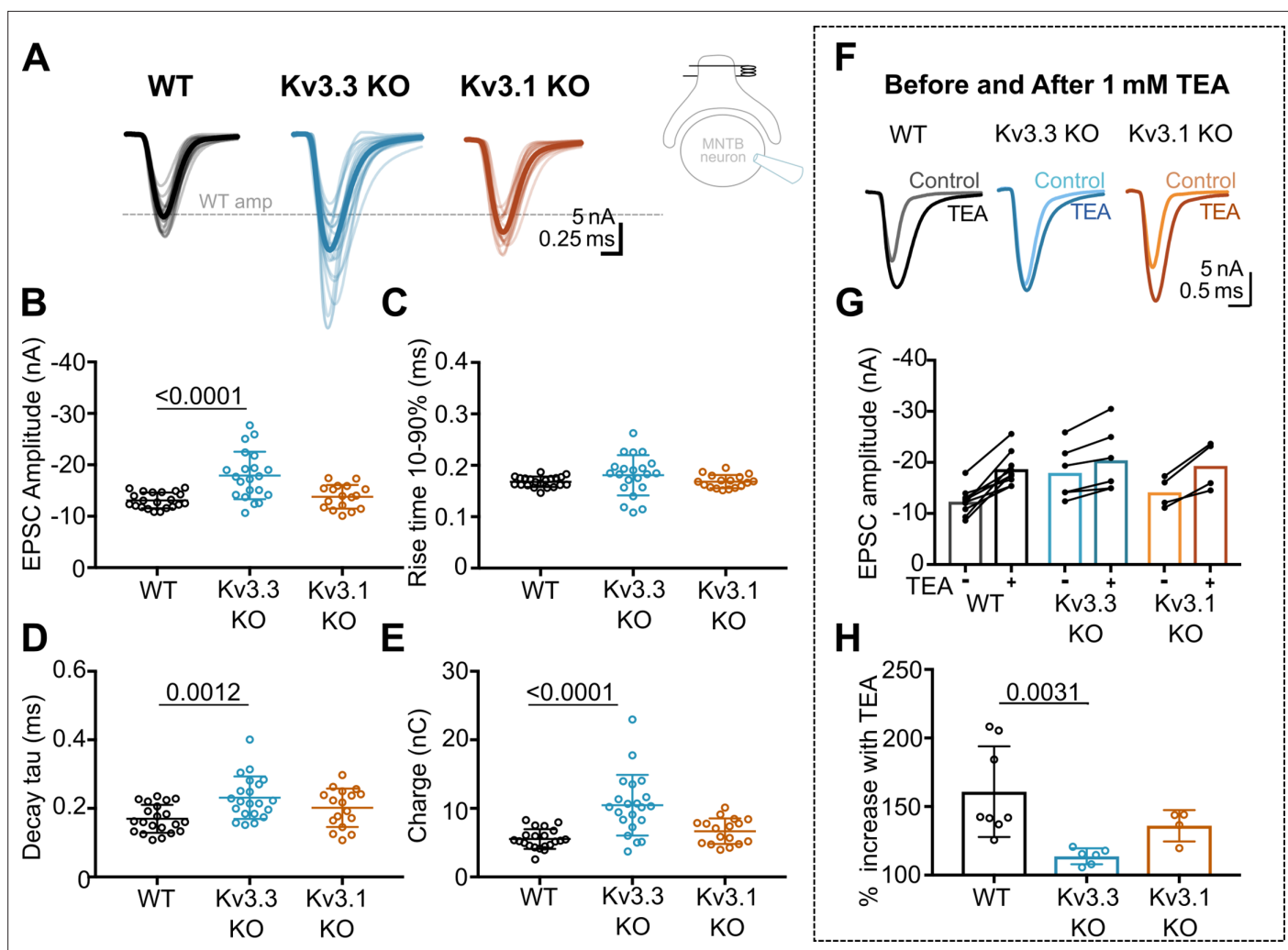
Figure 3. Kv3.3 deletion increases EPSC amplitude and occludes block by TEA. (**A**) Superimposed calyceal EPSCs generated from each genotype (age P21-P25): wildtype (WT; black), Kv3.3KO (blue), and Kv3.1KO mice (orange). Thin lines show traces from individual neurons (each is mean of 5 EPSCs) with thick line showing the population mean for each genotype. Grey dashed line indicates the average WT amplitude; N=WT, 22 neurons (11 mice); Kv3.3KO, 22 neurons (10 mice); Kv3.1KO, 17 neurons (8 mice). Inset shows recording and stimulation configuration. (**B**) EPSC amplitude increased in the Kv3.3KO. (**C**) EPSC rise time (10–90%) no difference was found between groups (one-way ANOVA, p=0.1576). (**D**) EPSC decay tau and (**E**) EPSC total charge were increased in the Kv3.3KO relative to WT. (**F**) EPSC traces from WT, Kv3.3KO, and Kv3.1KO mice, before and after the addition of 1 mM TEA. (Centre): EPSC amplitudes recorded before and after perfusion of TEA (1 mM); n=WT, 9 neurons (7 mice); Kv3.3KO, 6 neurons (3 mice); Kv3.1KO, 5 neurons (3 mice). (**G**) Increase in EPSC amplitude by 1 mM TEA. (**H**). The amplitude increase induced by TEA was significantly reduced in Kv3.3KO mice compared to WT. Average data presented as mean ± SD; statistics was using one-way ANOVA with Tukey's post hoc for multiple comparisons. Kruskal-Wallis ANOVA with Dunn's multiple corrections was used to compare change to EPSC amplitude in TEA due to a non-gaussian distribution in WT.

The online version of this article includes the following source data and figure supplement(s) for figure 3:

Source data 1. Relates to *Figure 3*.

Figure supplement 1. mEPSCs recorded from Kv3.3KO mice have a decreased amplitude.

Figure supplement 1—source data 1. Relates to *Figure 3—figure supplement 1*.

amplitude and longer lasting compared to WT or Kv3.1KOs, consistent with increased transmitter release from the calyx of Held in the Kv3.3KO.

The data for EPSC peak amplitude, rise-time, decay tau and charge are plotted in *Figure 3B–E*, respectively, for each genotype. EPSC amplitudes were similar in WT and Kv3.1KO, –13±2 nA (n=21) and –14±2 nA (n=17), respectively; but increased significantly in the Kv3.3KO to –18±5 nA (n=21; one-way ANOVA, Tukey's post hoc, Kv3.3KO vs WT, p=0.0001; Kv3.3KO vs Kv3.1KO p=0.0005). The decay tau for the EPSCs in the Kv3.3KO slowed to 0.23±0.06ms (n=21) compared to 0.17±0.04ms

in WT (n=21; one-way ANOVA, Tukey's post hoc, p=0.0012). The total charge of EPSCs in Kv3.3KOs increased to –10±4 nC (n=21) compared to –6±1 nC and –7±2 nC in WT (n=21) and Kv3.1KOs (n=17), respectively (one-way ANOVA, Tukey's post hoc; Kv3.3KO vs WT, p=0.0001; Kv3.3KO vs Kv3.1KO p=0.0007). No change of EPSC rise time was observed in either KO (one-way ANOVA, p=0.1918). Examination of miniature EPSCs in postsynaptic MNTB neurons from each genotype (*Figure 3—figure supplement 1*) showed no difference in the mEPSC frequency, rise-time or decay tau. There was a small significant decrease in quantal amplitude in the Kv3.3KO relative to WT, but no change in the Kv3.1KO. This contrasts with the increased amplitude of the evoked EPSCs in the Kv3.3KO measured here, and perhaps reflects an opposing change in synaptic scaling due to the larger transmitter release induced in the Kv3.3KO (*Tatavarty et al., 2013*).

The increased EPSC amplitude observed in Kv3.3KOs suggests that Kv3.3 subunits are major contributors to repolarisation of the presynaptic terminal. If Kv3.3 subunits dominate presynaptic Kv3 channels, then blocking presynaptic Kv3 channels with TEA will have a lesser effect on EPSCs from the Kv3.3KO. To test this hypothesis, we compared the effect of 1 mM TEA on EPSC amplitude from each of the three genotypes (*Figure 3F–H*). Indeed, blocking Kv3 channels with TEA had a much smaller effect on EPSC amplitude in the Kv3.3 KO compared to WT and Kv3.1 KO. TEA increased EPSC amplitude to 160% ± 33% (n=8) in WT, compared to 114% ± 6% (n=6) in Kv3.3KO (Kruskal-Wallis, Dunn's multiple comparison, p=0.0031). The EPSC amplitude in the Kv3.1KO (136% ± 11%, n=4) was not significantly different from WT (Kruskal-Wallis, Dunn's multiple comparison p=0.99). This result is consistent with dominance of presynaptic repolarisation by channels containing Kv3.3.

Enhanced short-term depression in Kv3.3KO

The calyx of Held/MNTB synapse is capable of sustained transmission at firing frequencies of around 300 Hz in vivo (*Kopp-Scheinpflug et al., 2008*) (also see Figure 8), encoding information about sound stimuli for binaural integration with high temporal precision. Indeed, the calyx of Held giant synapse can sustain short AP bursts with peak firing rates of up to 1000 Hz, in vitro (*Kim et al., 2013*) for a few milliseconds. Clearly, the increased transmitter release observed in the Kv3.3KO (*Figure 3*) has consequences for maintenance of EPSC amplitude during repetitive firing, in that vesicle recycling and priming must rapidly replace docked vesicles if transmitter release is to be maintained for the duration of the high frequency train. Repetitive stimulation shows that the evoked EPSC amplitude declines during a stimulus train until rates of vesicle priming are in equilibrium with the rate of transmitter release for a given stimulus frequency. To assess repetitive transmitter release in each of the genotypes we evoked EPSCs over a range of frequencies from 100 to 600 Hz (with each stimulus train lasting 800ms).

Whole-cell patch recordings from voltage-clamped MNTB neurons (HP = –40 mV) were conducted in which calyceal EPSC trains were evoked at 100 Hz, 200 Hz, or 600 Hz. Each train was repeated three times, with a resting interval of 30 s between repetitions of stimuli trains. The EPSC amplitudes during the trains were compared in MNTB neurons of each genotype: WT (black), Kv3.3KO (blue) and Kv3.1KO (orange) mice. The first EPSC amplitude in trains delivered to the calyx/MNTB from the Kv3.3KO mouse was of larger amplitude than observed in WT or in the Kv3.1KO and subsequent EPSCs showed a larger short-term depression. In *Figure 4A–C* a matrix of EPSC trains are plotted with the same stimulus frequency in each row for each genotype. The inset traces show the first 3 EPSCs and the last 3 EPSCs in each train, with the black arrow heads indicating the WT amplitude for comparison across genotypes.

Paired pulse ratio (PPR) was significantly decreased in the Kv3.3KO compared to both WT and Kv3.1KO at 100 Hz, 200 Hz, and 600 Hz, with mean PPR ($EPSC_2/EPSC_1$) plotted in *Figure 4D* (left column). This enhanced depression of EPSC amplitude was maintained for the duration of the train shown in comparison with the 80th EPSC in the train ($EPSC_{80}/EPSC_1$; *Figure 4D*, right column; *Table 1*).

The mean data, normalized to the amplitude of the first EPSC, is plotted for each genotype at the stated stimulus frequency: *Figure 4E–G* (100–600 Hz). There are two key parameters plotted below each depression curve: first, the short-term depression decay time-constant (Decay Tau, defined as the rate at which the EPSC amplitude equilibrates to the new steady-state amplitude at each stimulus frequency); and second, amplitude at steady-state (the amplitude of the new steady-state EPSC during the train, relative to $EPSC_1$). The Kv3.3KO consistently showed the fastest rate of short-term depression, compared to WT and Kv3.1KOs; this was highly significant at 100 Hz and 200 Hz (*Table 1*).

Figure 4. Evoked EPSC short-term depression is faster and more pronounced in the Kv3.3KO. (**A,B,C**) Example MNTB EPSC trains (800ms) on stimulation at (**A**) 100, (**B**) 200 or (**C**) 600 Hz for WT (left, black), Kv3.3KO (middle, blue), and Kv3.1KO (right, orange) mice (aged P21-P25). Each trace shows an average of 5 trials from a single neuron with stimulus artefacts removed for clarity. Lower insets: The first and last three EPSC traces are shown below each train. Black arrows show EPSC amplitudes from the WT mouse (left). Vertical grey arrows indicate multiple, asynchronous responses in the final EPSCs of Kv3.3KO traces. (**D**) Paired-pulse ratios for $EPSC_2/EPSC_1$ (left) and $EPSC_{80}/EPSC_1$ (right) generated in response to 100 Hz (top), 200 Hz (middle), and 600 Hz (bottom); in each case the ratio is significantly decreased in Kv3.3KO with respect to WT. For 100 Hz - WT: N=21 cells (11 mice); Kv3.3KO: N=21 (10 mice); Kv3.1KO: N=17 (8 mice); for 200 and 600 Hz - WT: N=10 (6 mice); Kv3.3KO: N=9 (4 mice); Kv3.1KO: N=5 (3 mice). Data shows mean ± SD and statistical significance estimated by one-way ANOVAs with Tukey's post hoc for multiple comparisons or Kruskal-Wallis with Dunn's multiple comparison ($EPSC80/EPSC1$ at 100 and 200 Hz due to non-gaussian data distributions), significant P values given on the respective graphs. (**E, F, G**) Normalised EPSCs, short-term depression is faster and larger in Kv3.3KO mice (compared to WT and Kv3.1KO mice) (**E**) 100 Hz F: 200 Hz G: 600 Hz. The rate of EPSC depression is plotted as a single exponential tau (lower left) and normalised EPSC amplitudes at steady-state are plotted (lower right) for each genotype and stimulus frequency. N numbers are presented in brackets on normalised EPSC amplitude graphs (and are the same neurons as

Figure 4 continued on next page

Figure 4 continued

used in D). One-way ANOVAs with Tukey's post hoc for multiple comparison correction were used to test significance, p values reported on graphs. All data plotted as mean ± SD, except in graphs of normalised EPSC amplitudes (E, F, and G, top) where data is plotted as mean ± SEM for clarity.

The online version of this article includes the following source data for figure 4:

Source data 1. Relates to *Figure 4*.

This trend continued so that during stimuli at 600 Hz (*Figure 4G*), a further increase in the rate of short-term depression was observed; again, this was most marked in EPSC trains from the Kv3.3KO compared to both WT and Kv3.1KO. The decay time-constant for short-term depression was 6±1ms for Kv3.3KOs (n=8), 11±2ms for WT (n=10) and 20±13ms for Kv3.1KOs (n=5; *Table 1*).

Following short-term depression, the 'steady-state' EPSC amplitude was achieved after 20–40 evoked responses (*Figure 4E, F and G*; lower right graph). This reflects the net equilibrium achieved under control of four key presynaptic parameters: probability of transmitter release, the rate of AP stimulation, the rate of vesicle replenishment at the release sites and the size of the vesicle pool (see modelling section below). In young animals, postsynaptic AMPAR desensitisation can also play a role in short-term depression, but this is a minor contribution at mature synapses and physiological temperatures, as employed here (*Taschenberger et al., 2002*; *Wong et al., 2003*). At all frequencies, EPSCs from the Kv3.3KO mice showed lower amplitude steady-state values in comparison to WT; while the Kv3.1KO data was either the same or greater than WT (*Figure 4E*, *Table 1*).

Table 1. Short-term depression was accelerated and enhanced in mice lacking Kv3.3.

Values shown are for parameters measured from data presented in *Figure 3* for WT, Kv3.3KO and Kv3.1KO genotypes at 100 Hz to 600 Hz range. Paired pulse depression of EPSC responses recorded in MNTB neurons ($EPSC_2/EPSC_1$) was increased in Kv3.3 KO animals during high frequency stimulation of the calyx. The increased depression was maintained throughout the stimulation train ($EPSC_{80}/EPSC_1$) across all frequencies. The rate of short term-depression in EPSC amplitudes during EPSC trains (duration 800ms), measured as short-term depression (STD) decay tau was significantly increased in Kv3.3 KOs at 100 and 200 Hz compared to WT. This STD was more severe in mice lacking Kv3.3, as shown by decreased normalized steady-state EPSC amplitudes compared to WT. STD tau and steady state amplitudes were measured using a single exponential fit to normalized EPSC amplitudes throughout the 800ms stimulation trains. n=number of neurons. Values in bold are significantly different to WT (see statistics table for more detail). Data represented as mean ± SD.

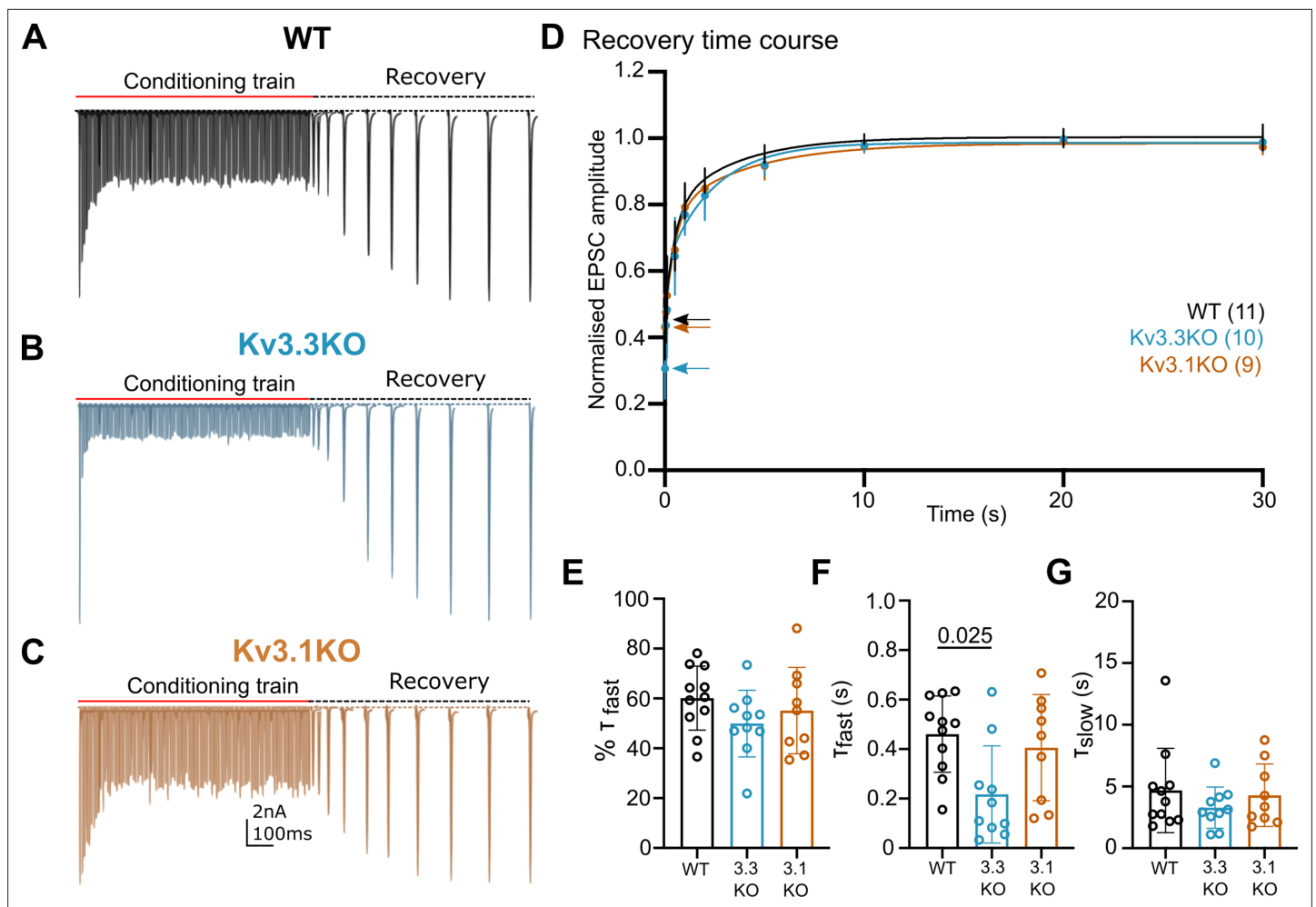|		WT	Kv3.3KO	Kv3.1KO
	$EPSC_2/EPSC_1$ Ratio	0.90±0.04 (n=21)	**0.75±0.08 (n=21)**	0.92±0.06 (n=17)
	$EPSC_{80}/EPSC_1$ Ratio	0.45±0.13 (n=21)	**0.32±0.08 (n=21)**	0.55±0.19 (n=17)
	STD tau (ms)	41±7 (n=21)	**24±5 (n=21)**	45±2 (n=17)
100 Hz	Norm. steady-state amp	0.4±0.1 (n=21)	**0.3±0.08 (n=21)**	**0.6±0.2 (n=17)**
	$EPSC_2/EPSC_1$ Ratio	0.90±0.03 (n=10)	**0.71±0.1 (n=9)**	0.93±0.05 (n=5)
	$EPSC_{80}/EPSC_1$ Ratio	0.34±0.10 (n=10)	**0.22±0.03 (n=9)**	0.56±0.20 (n=5)
	STD tau (ms)	25±6 (n=10)	**13±4 (n=9)**	**33±5 (n=5)**
200 Hz	Norm. steady-state amp	0.3±0.10 (n=10)	**0.2±0.03 (n=9)**	0.5±0.1 (n=5)
	$EPSC_2/EPSC_1$ Ratio	0.91±0.06 (n=8)	**0.68±0.10 (n=9)**	0.91±0.15 (n=6)
	$EPSC_{80}/EPSC_1$ Ratio	0.25±0.19 (n=8)	**0.1±0.02 (n=9)**	0.18±0.042 (n=6)
	STD tau (ms)	7±5 (n=7)	3±1 (n=6)	5±2 (n=4)
400 Hz	Norm. steady-state amp	0.26±0.12 (n=6)	**0.12±0.04 (n=7)**	0.12±0.04 (n=3)
	$EPSC_2/EPSC_1$ Ratio	0.8±0.08 (n=10)	**0.7±0.1 (n=8)**	0.9±0.07 (n=5)
	$EPSC_{80}/EPSC_1$ Ratio	0.15±0.04 (n=10)	**0.09±0.01 (n=8)**	0.16±0.07 (n=5)
	STD tau (ms)	11±2 (n=10)	6±1 (n=8)	20±13 (n=5)
600 Hz	Norm. steady-state amp	0.11±0.03 (n=10)	**0.07±0.01 (n=8)**	0.11±0.02 (n=5)

Figure 5. Recovery from short-term depression is accelerated on deletion of Kv3.3. (**A**) WT (black),(**B**) Kv3.3KO (blue),(**C**) Kv3.1KO (orange). A representative example is shown for each genotype. A conditioning train of 100 Hz (800ms duration) evoked EPSCs displaying short-term depression. The recovery was estimated by delivery of single stimuli at intervals following the conditioning train (50ms, 100ms, 500ms, 1 s, 2 s, 5 s, 10 s, 20 s, and 30 s. Recovery intervals not to scale).(**D**) The mean EPSC amplitude during the recovery is plotted for each genotype (mean ± SD. WT, black; Kv3.3KO, blue; Kv3.1KO, orange) over the 30 s recovery period. The mean amplitude at the end of the conditioning train, from which the recovery starts, is shown by the respective coloured arrow. A double exponential was fit to each individual recovery curve and the mean curve is plotted for the respective genotype. Values are plotted as raw data and mean ± SD in E-G; N values from part D also apply here. (**E**) The percent contribution of the fast component is similar between genotypes. (**F**) The fast time-constant significantly accelerated from 0.4 s in WT to 0.2 s in the Kv3.3KO. (**G**) The slow time-constant at around 5 s was unchanged between genotypes.

The online version of this article includes the following source data for figure 5:

Source data 1. ,Relates to *Figure 5*.

Kv3.3 deletion accelerated a fast component of recovery from short-term depression

Presynaptic spike broadening has previously been shown to enhance vesicle recycling during repetitive stimulation trains (*Wang and Kaczmarek, 1998*) due to enhanced calcium-dependent recovery. An increase in the rate of recovery of the evoked EPSC following short-term depression (*Figure 5*) could indicate changes in vesicle recycling. In WT animals the EPSC was depressed to around 40% on stimulation at 100 Hz (*Figure 4E*), increasing to 90% depression for 600 Hz (*Figure 4G*). Three example conditioning traces are shown in *Figure 5A–C* for each genotype. On ceasing stimulation, the depressed EPSC recovered back to control amplitudes over a time-course of 30 s (*Figure 5A–C*, recovery). The recovery phase was measured by presenting stimuli at intervals of: 50, 100, 200, 500 ms, and 1, 2, 5, 10, 20, and 30 s after the end of the conditioning train. Each recovery curve was

repeated 3 times and the mean EPSC amplitudes plotted over the 30 s period (*Figure 5D*) and fit with a double exponential. The fast time-constant contributed around half of the recovery amplitude and this did not differ significantly between the three genotypes (*Figure 5E*). The fast time-constant was significantly accelerated in the Kv3.3KO compared to WT and Kv3.1KO (0.2±0.2 s in Kv3.3KO; 0.45±0.2 s in WT and 0.4±0.2 s in the Kv3.1KO; *Figure 5F*, p=0.025). The slow time-constant was 5±3 s in WT, and was similar to both Kv3.1KO and Kv3.3KO (*Figure 5G*). The enhanced fast recovery rate is consistent with an activity-dependent component of vesicle recycling as observed previously on blocking presynaptic Kv3 channels at the calyx of Held (*Wang and Kaczmarek, 1998*) and as recently attributed to Ca^{2+}-phospholipid-dependent vesicle priming (*Lipstein et al., 2021*) via Munc13-1.

Computational model of transmitter release

The magnitudes and rates of EPSC depression and recovery following synaptic train stimulation provided constraints in refining a computational model of transmitter release and vesicle recycling at the calyx of Held (*Graham et al., 2004*). A simple model of transmission at the calyx of Held, based on transmitter release and recycling was employed as set out in *Figure 6A*, *equations 1-3*. It included activity-dependent vesicle recycling (*Graham et al., 2004*; *Billups et al., 2005*; *Lucas et al., 2018*) and parameters were fit across the range of stimulus frequencies (100–600 Hz) for the WT and the Kv3.3KO mouse. The model possessed a readily releasable pool (RRP; normalized size n), from which vesicles undergo evoked exocytosis with a release probability (Pv), following each AP and are recycled with a time-constant τ_r. A basal rate of recycling (large time-constant τ_b) is accelerated to an activity-dependent rate (smaller time-constant τ_h) on invasion of an AP, and relaxed back to τ_b with a time-constant of τ_d. The table in *Figure 6B* shows that the dominant change in the model parameters between WT and Kv3.3KO, was an increase in the probability of vesicular release (Pv) from 0.13 in WT to 0.266 in the Kv3.3KO. There was also evidence for an increase in activity-dependent recycling, with a 20% acceleration of the replenishment rate (smaller τ_h in Kv3.3KO). The fit of the model to the mean experimental data (± SEM) is shown for the short-term depression and the recovery curves (WT: *Figure 6C–D*; Kv3.3KO: *Figure 6E–F*). This model showed that the physiologically observed changes in short-term depression and recycling could be fit across the range of stimuli rates with only two parameter changes in the Kv3.3KO: a dramatically increased Pv and a modest decrease in the activity-dependent vesicle recycling time-constant τ_h (higher recycling rate), both of which are attributable to the raised calcium influx during the presynaptic AP (see *Neher and Sakaba, 2008*; *Young and Veeraraghavan, 2021*).

Integration of EPSCs in generating APs in the postsynaptic MNTB neuron

A key physiological question is the extent to which presynaptic Kv3.3 influences AP firing of the MNTB neuron in response to trains of synaptic stimuli, since most auditory stimuli will be trains rather than single APs. This was addressed in two experiments: first in an in vitro slice study comparing the AP firing of MNTB neurons in response to synaptic stimulation over a range of frequencies and across the genotypes (*Figure 7*) and then through an in vivo study of the response of MNTB neurons to sound-evoked inputs, focusing on the Kv3.3KO and WT genotypes (*Figure 8*).

The first question was how does MNTB AP firing in response to a train of synaptic inputs change on deletion of Kv3.1 and Kv3.3? The initial observation was that MNTB AP output in response to high frequency calyceal EPSC input, declines with both Kv3.1 and Kv3.3 deletion (*Figure 7A*) when measured over the whole train (WT: 52.49% ± 8.15%, n=5; Kv3.3KO: 29.8% ± 10.43%, n=7; Kv3.1KO: 36.29% ± 11.12%, n=6; Kv3.3KO vs WT p=0.0044, Kv3.1KO vs WT p=0.046, one-way ANOVA, Tukey's post hoc). But closer inspection reveals three phases of AP firing to evoked trains of calyceal synaptic responses as illustrated in *Figure 7B*. This shows MNTB EPSPs/APs during an 800ms 600 Hz train in a WT mouse. In Phase I (green trace, *Figure 7B*) which predominates at the start of each train, every evoked EPSP triggered one MNTB AP: so the MNTB output matched the calyx input. Firing then transitioned to Phase II (blue trace, *Figure 7B*) after around 6–9 stimuli, where EPSPs often failed to evoke an AP, and the MNTB AP firing becomes chaotic, unpredictable and poorly transmits the timing information contained within the presynaptic AP train. In Phase III (black trace, *Figure 7B*): the EPSP had undergone short-term depression and approached a 'steady-state' amplitude; now the MNTB neuron fired APs to alternate EPSPs. At frequencies up to 200 Hz the duration of Phase I was essentially
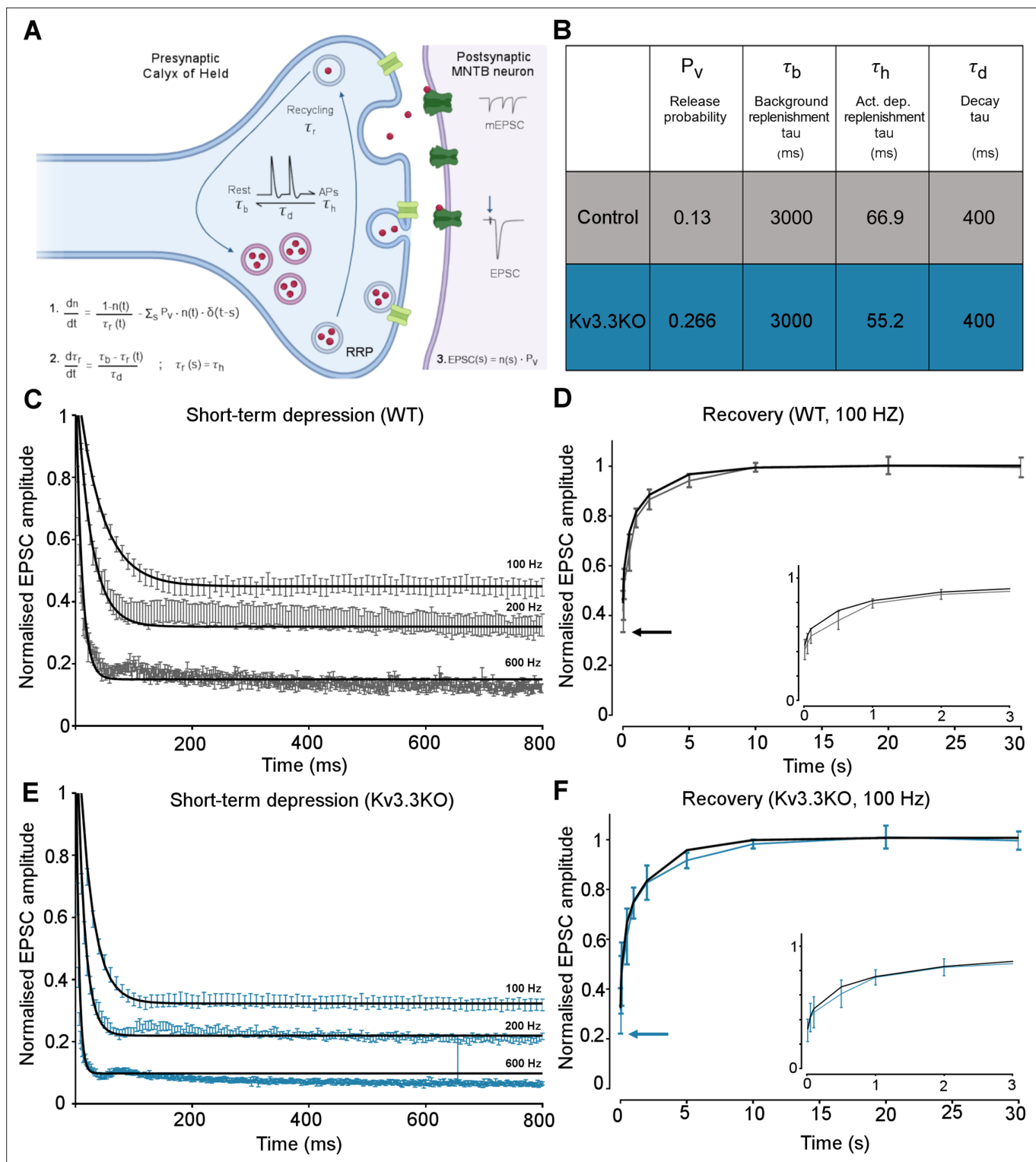
Figure 6. Kv3.3 deletion increases release probability and speeds a fast component of vesicle recycling, based on computational modelling. (**A**) Model illustration: Vesicles are released from the readily releasable pool (RRP; normalized size n) with a probability Pv; the RRP is replenished with the recycling time-constant t_r. In the absence of APs $\tau_r = \tau_b$ – the background replenishment time-constant, which decreases (accelerates) to τ_h following a presynaptic AP, and decays back to τ_b with a time-constant τ_d. Model parameters were fit to WT data for evoked EPSC trains (100–600 Hz) and their 100 Hz recovery curves. Schematic created with BioRender.com. (**B**) Table showing the model parameters for fitting WT and Kv3.3KO data. Increasing Pv from 0.13 to 0.266 and accelerating τ_h from 66.9 to 52.2 were sufficient to fit the changes observed on Kv3.3 deletion. (**C**) WT - EPSC amplitude data (mean ± SEM) during the conditioning train (100, 200, and 600 Hz, grey) are plotted with superimposed model prediction curves (black). (**D**) WT

Figure 6 continued on next page

Figure 6 continued

100 Hz: Recovery of the EPSC (mean ± SEM) over 30 s. Inset shows data and fit for the first 3 s. Model fit is the superimposed black line. Horizontal arrow indicates EPSC amplitude at the end of the conditioning train. (**E**)Kv3.3KO: EPSC amplitude data (mean ± SEM) during the conditioning trains are plotted (blue) with superimposed model prediction curves (black). (**F**) Kv3.3KO 100 Hz: Recovery of the EPSC amplitude (mean ± SEM) over 30 s. Inset shows data and fit for the first 3 s. Model fit is the superimposed line. Horizontal arrow indicates EPSC amplitude at the end of the conditioning train.

The online version of this article includes the following source data for figure 6:

Source data 1. Relates to *Figure 6*.

identical across the three genotypes (*Figure 7C*), all showed 100% firing throughout the train; then from 300 Hz and above, the Phase I duration declined dramatically for all genotypes. Genotype-specific limitations were observed at the highest frequencies. *Figure 7D* shows the relative duration of each phase for 600 Hz EPSP trains (as a % of the train duration). There were no differences in the duration of Phase I, while Phase II and III were of variable duration. At 600 Hz stimulation frequency, the latency to the start of Phase II was 34.3±12.3ms for WT (n=10), 25±8ms for Kv3.3KO (n=6) and 26±14ms for Kv3.1KO (n=5). The latency for Phase III was similar in WT and Kv3.1KO (510±224ms and 597±251ms, respectively) but in the Kv3.3KO only 1 out of 6 calyx/MNTB pairs briefly entered Phase III firing (Kv3.3KO vs WT Phase II p=0.0135, Phase III p=0.02, two-way ANOVA, Tukey's post hoc). This is consistent with the idea that presynaptic Kv3.3 and hence fast presynaptic APs, serve a role in maintaining information transmission across the synapse during high frequency firing, when short APs conserve resources, and slow the rate of short-term depression.

Large magnitude Kv3 currents in postsynaptic MNTB neurons demonstrably assists in transmission of timing information (*Song et al., 2005*). Kv3 has little impact on the resting MNTB neuron membrane time-constant or AP firing threshold (induced by current injection through the pipette) and these are essentially identical in the three genotypes (*Choudhury et al., 2020*), which was also confirmed here (*Figure 7i*). However, in the Kv3.1KO, calyceal stimulation evoked a sustained depolarisation (in addition to EPSPs) at frequencies above 100 Hz (*Figure 7E*). The mean amplitude of this depolarising plateau potential during the train is plotted against stimulus frequency for each genotype (*Figure 7F*). Although all genotypes exhibited this plateau depolarisation at 600 Hz, it was significantly larger for the Kv3.1KO at frequencies above 100 Hz (*Figure 7F*). In contrast, Kv3.3KOs showed a reduced plateau potential at frequencies above 300 Hz, reaching significance only at 600 Hz (*Figure 7F*; two-way ANOVA, Tukey's post hoc). This was also observed as a decaying depolarisation at the end of the train (*Figure 7G*), with the time to half-decay plotted in *Figure 7H* (WT: 2.79±1.73ms, n=7: Kv3.3KO: 1.89±0.92ms, n=6: Kv3.1KO: 15.96±8.59ms, n=8: Kv3.1KO vs WT p=0.000553, one-way ANOVA, Tukey's post hoc). In WT and Kv3.3KO genotypes, this decay was similar to the postsynaptic membrane time-constant, but in the Kv3.1KO, non-synchronous spontaneous EPSPs were observed. The EPSC decay time constants for all genotypes were essentially identical, consistent with no change in glutamate receptor expression (WT: 2.74±1.26ms, n=8; Kv3.3KO: 3.1±0.87ms, n=8; Kv3.1KO: 3.54±0.9ms, n=6). This plateau depolarisation caused increased depolarisation block of APs and thereby undermined our ability to examine AP firing physiology in the Kv3.1KO. Therefore, in vivo experiments focused on comparison of the WT and Kv3.3KO genotypes, which did not exhibit this postsynaptic epi-phenomenon.

Kv3.3 increases precision and signal-to-noise ratios in MNTB response to sound

The prolonged presynaptic AP duration and increased transmitter release observed here in the Kv3.3KO, shows that the calyx has a specific need for Kv3.3 channels. So, what is the impact of presynaptic Kv3.3 on brainstem auditory processing in the MNTB?

Behaviourally, the Kv3.3KO mouse is as sensitive to sound as the WT in that Auditory Brainstem Response (ABR) thresholds were similar in 6-month-old WT and Kv3.3KO mice, with no statistical difference across a wide frequency range (see summary statistics, unpaired t-test with Holm-Šídák's test for multiple comparisons). However, further analysis of the ABR waveform showed significant deficits in Wave IV at 6 months which were not apparent in recordings taken at 1 month of age. We have previously demonstrated that a developmental 'knockout' of the MNTB impacts ABR Wave III (*Jalabi et al., 2013*), so the decrease in Wave IV reflects changes in downstream areas of the auditory
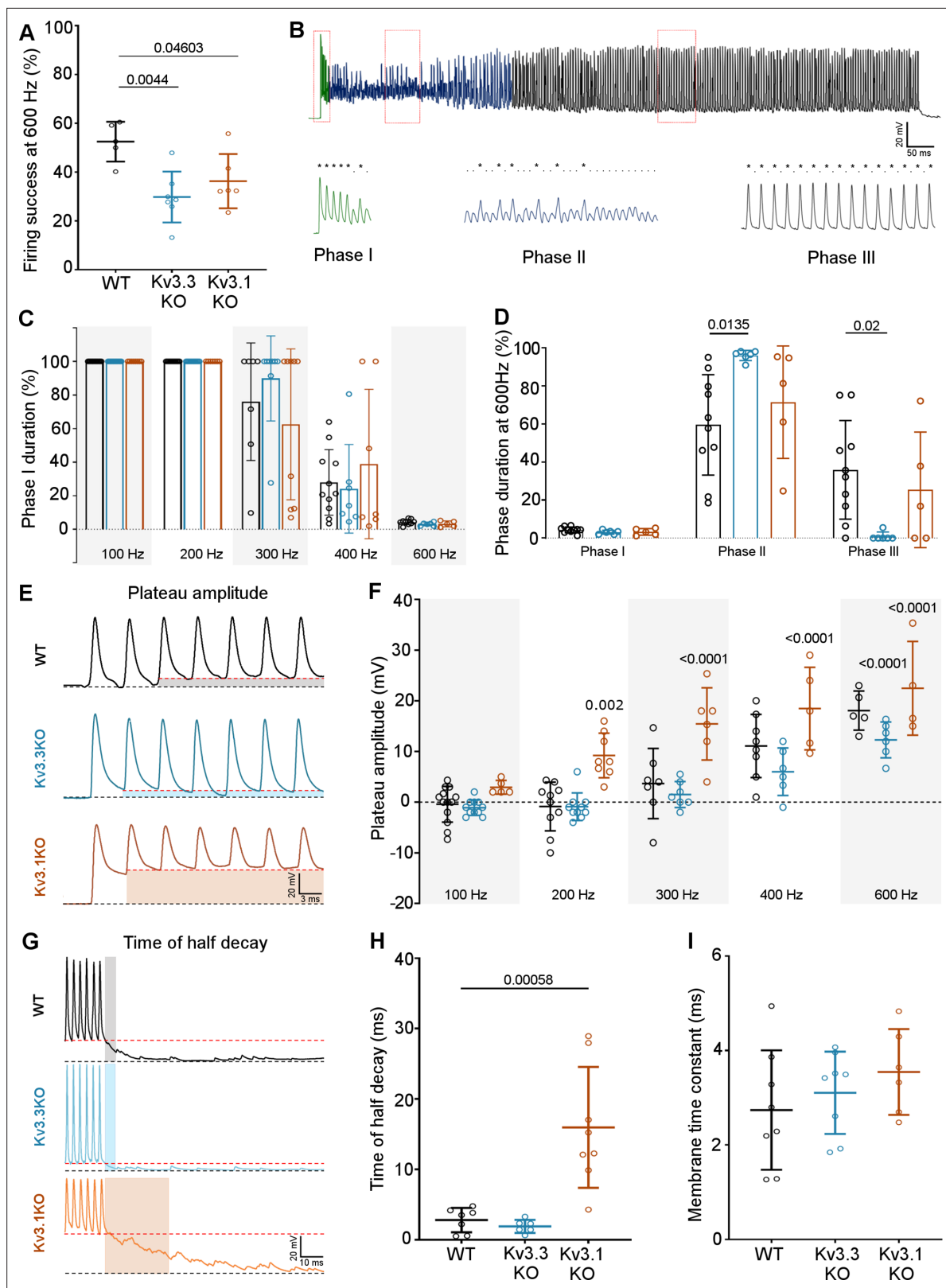
Figure 7. Kv3.3 deletion reduced ability to sustain MNTB AP firing at high frequencies. (**A**) Percent firing success of MNTB neurons for 600 Hz calyceal stimulation is reduced for both Kv3.3KO and Kv3.1KO.(**B**) A representative AP train recorded for an MNTB neuron in response to 600 Hz synaptic stimulation lasting 800ms. Three phases of input:output firing defined: Phase I (green) 1:1 AP firing calyx:MNTB for each EPSC is prevalent early in the train. Phase II (dark blue) follows phase I where some EPSCs drop below threshold, and AP firing becomes less probable and chaotic. Phase III (black)

Figure 7 continued on next page

Figure 7 continued

MNTB AP firing becomes regular again but is now firing to alternate input EPSCs, restoring information transmission. Expanded sections (boxed) of each phase of AP firing are shown below the full trace, APs are indicated by '*' and EPSPs that are below threshold are indicated by '.'. (**C**) Phase I duration across stimulation frequencies (100–600 Hz) for each genotype (WT, black; Kv3.3KO, blue; Kv3.1KO, orange): Phase I firing lasts throughout the train at frequencies up to 300 Hz but declines to only a few milliseconds at 600 Hz synaptic stimulation, but there were no significant differences between the genotypes. (**D**) The time spent in each phase for 600 Hz stimulation train (with each genotype indicated by the same colours as in C). The MNTB neuron is unable to maintain Phase I and Phase II dominates for each genotype. However, Phase III is only achieved briefly on 1 of 6 observations in the Kv3.3KO.(**E**) A sustained depolarized plateau was also observed, in the MNTB AP trains, as indicated by the shaded regions in this data from 300 Hz, and was particularly large the Kv3.1KO. (**F**) The amplitude of the depolarisation plateau increased in magnitude with stimulation frequency for each genotype, but was significantly larger in the Kv3.1KO at all frequencies above 100 Hz. (**G**) A slowly decaying depolarisation following the end of the synaptic train, as shown for representative traces from each genotype. (**H**) This decaying depolarisation is quantified as the time to half-decay and was significantly longer in the Kv3.1KO compared to WT in a 300 Hz AP train. (**I**) The postsynaptic MNTB neuron membrane time constant was unchanged across all genotypes (genotype: WT, black; Kv3.3KO, blue; Kv3.1KO, orange).

The online version of this article includes the following source data for figure 7:

Source data 1. Relates to *Figure 7*.

brainstem and is being characterized as part of another study. Here, we used the opportunity to examine auditory processing in the MNTB in vivo using extracellular recordings from WT and Kv3.3KO mice during sound stimulation. This data was non-gaussian and summary statistics are presented as median, and quartile values (in square brackets).

Extracellular MNTB single unit recordings exhibited a typical complex waveform, comprised of a presynaptic and a postsynaptic component (*Figure 8A*; *Kopp-Scheinpflug et al., 2003*). The time between the peak and trough of extracellular APs is a compelling marker for AP halfwidth (*Ritzau-Jost et al., 2021*) and confirmed our results of the presynaptic patch clamp recordings. AP halfwidth of the presynaptic AP (preAP) was significantly longer in Kv3.3KOs (0.25ms [0.16; 0.31]; n=13) compared to WT recordings (0.17ms [0.16; 0.19]; n=20; *Figure 8B*; Mann-Whitney Rank Sum Test: p=0.036). Synaptic delays as measured by peak-to-peak times in the complex waveform were also significantly prolonged in Kv3.3KOs (0.56ms [0.45; 0.70]; n=13) compared to WT controls (0.44ms [0.41; 0.49]; n=20; *Figure 8C*; n=13; Mann-Whitney Rank Sum Test: p=0.013). While changes in presynaptic AP duration and synaptic delay may predominantly affect temporal processing, the prolonged postsynaptic AP duration observed in the Kv3.3KOs (0.64ms [0.29; 0.46]; n=13; *Figure 8D*) might influence high-frequency firing abilities (WT: 0.36ms [0.48; 0.82]; n=20; Mann-Whitney Rank Sum Test: p≤0.001).

Temporal processing was tested by presenting suprathreshold sound stimuli at the neurons' characteristic frequency in 6–8 months old mice and comparing WT and Kv3.3KO strains. MNTB neurons in WT responded with a phasic-tonic firing pattern (*Figure 8E and F*) with short latencies (3.44ms [3.01; 4.21]; n=25; *Figure 8I and J*) and minimal jitter (0.18ms [0.09; 0.51]; n=18; *Figure 8I and K*). In contrast, Kv3.3KO neurons were slower to respond to sound with first spike latencies of 4.06ms [3.01; 4.21] (n=25; Mann-Whitney Rank Sum Test: p=0.015; *Figure 8I and J*) and showed larger temporal variability (0.92ms [0.56; 1.50]; n=18; Mann-Whitney Rank Sum Test: p=0.001; *Figure 8I and K*). This increased onset jitter contributed to the reduced magnitude of the phasic component in the peri-stimulus time histogram in Kv3.3KO neurons (*Figure 8F* arrows). The inability to fire high instantaneous rates at sound onset was accompanied by a shift in the average inter-spike intervals from 2.16ms [1.48; 3.57] (n=22) in the WT to 3.10ms [2.49; 4.19] (n=18) in the Kv3.3KO (Mann-Whitney Rank Sum Test: p≤0.001; *Figure 8G*). Indeed, comparing peak firing rates during the first 10ms of the sound-evoked response revealed significantly lower rates in Kv3.3KOs (240 Hz [180; 280]; n=18) compared to WTs (350 Hz [200; 425]; n=22; Mann-Whitney Rank Sum Test: p=0.003; *Figure 8H*). In contrast to the reduced sound-evoked firing rates, an increase in spontaneous firing was observed in the Kv3.3KOs (Kv3.3KO: 40 Hz [19.3; 62.0]; n=19) compared to WT controls (16.5 Hz [4.5; 42.8]; n=24; Mann-Whitney Rank Sum Test: p=0.044; *Figure 8L*). Together, these combined changes caused a significant reduction in signal-to-noise ratio in the Kv3.3KO (2.77 [2.04; 3.99]; n=14) compared to WT controls (9.70 [4.38; 40.95]; n=18; Mann-Whitney Rank Sum Test: p=0.001; *Figure 8M*).
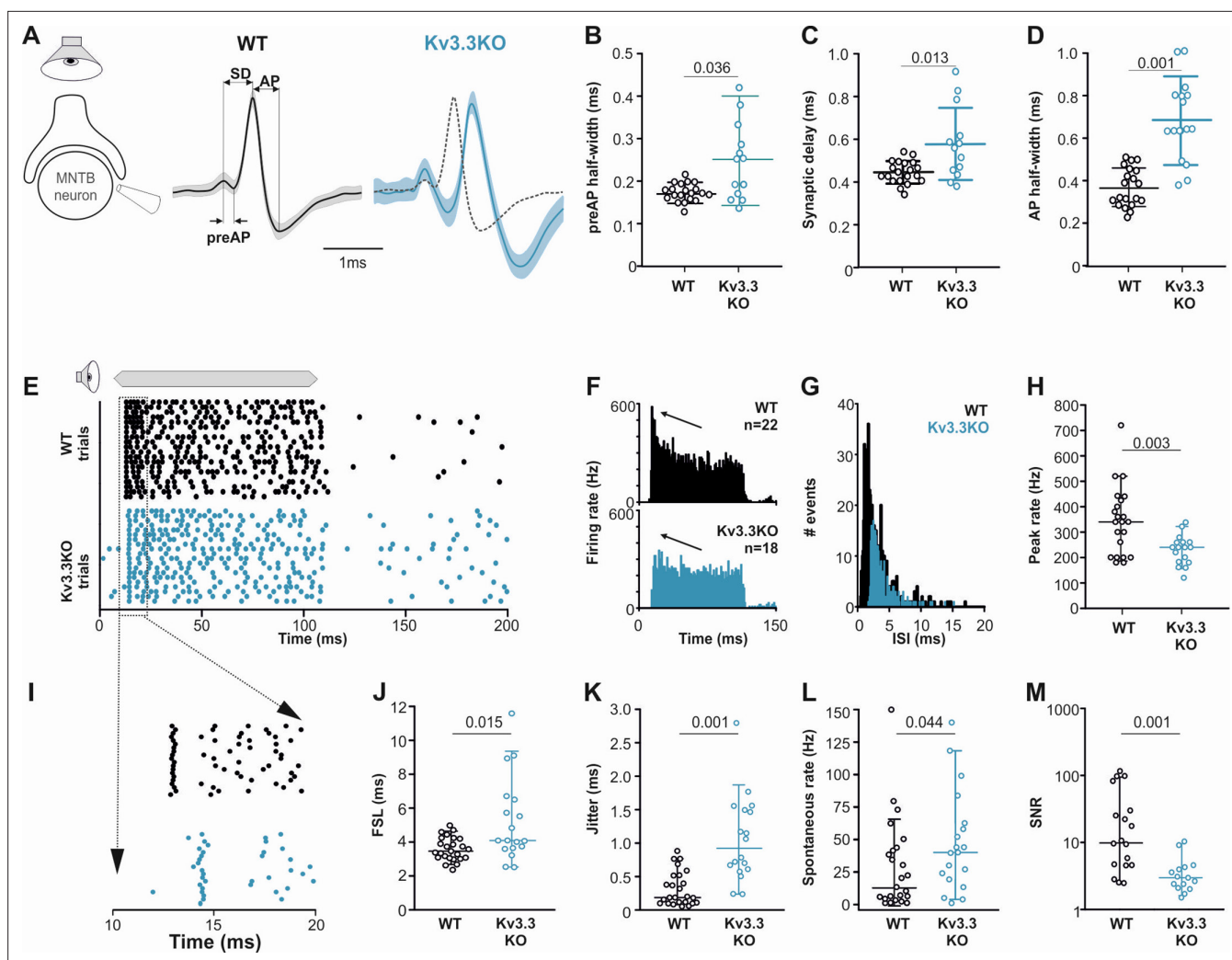
Figure 8. Presynaptic Kv3.3 accelerates the brainstem response to sound and improves timing and signal-to-noise ratio. (**A**) Extracellular recording from Calyx/MNTB in vivo shows complex APs (presynaptic and postsynaptic) from WT (black) and Kv3.3KO (blue) mice in response to sound; overlay of APs (right) shows delayed and longer APs in the KO. (**B, C, D**) Presynaptic AP half-width, synaptic delay and postsynaptic AP half-width are all longer in the Kv3.3KO (blue) than WT (black).(**E**) Raster display of MNTB AP response to sound (20 trials, 100ms duration) and spontaneous firing for both WT (black, upper) and Kv3.3KO (blue, lower). (**F, G, H**) Peri Stimulus Time Histogram (PSTH) of the evoked APs (grand avg. over all neurons, 1ms bins) show reduced peak firing rates (F, black arrow) due to longer interspike intervals (ISIs) and increased jitter (**I, K**) in the Kv3.3KO (blue) and the peak (0–10ms of the response) firing rate is significantly reduced. (**I, J, K**) Expansion of first 20ms of the Raster plot shows increased first spike latency and jitter (latency SD) in the Kv3.3KO (blue). (**L, M**) The mean spontaneous firing rate was higher in the Kv3.3KO (blue) and overall, these changes degraded signal-to-noise ratio in Kv3.3KO (blue) relative to WT (black). Data is presented as median and inter-quartiles. p Values calculated using Mann-Whitney Rank Sum Test and statistically significant values displayed on each graph.

The online version of this article includes the following source data for figure 8:

Source data 1. Relates to *Figure 8*.

Discussion

Neurotransmitter release is triggered by calcium influx through voltage-gated calcium channels and is highly influenced by the presynaptic AP waveform. Deletion of Kv3.3 subunits increased presynaptic AP duration and transmitter release, enhancing short-term depression on repetitive stimulation. In contrast, deletion of Kv3.1 had little effect on the presynaptic AP or transmitter release. Expansion microscopy was used to enhance resolution in imaging presynaptic compartments and showed localisation of Kv3.3 subunits to the presynaptic membrane. These observations are consistent with a computational model of transmitter release in which Kv3.3 deletion increased vesicle release probability by twofold and to a lesser degree accelerated fast vesicle replenishment. This is consistent with

increased calcium influx and activity-dependent facilitation of recycling. The enhanced short-term depression of synaptic responses increased latency jitter and reduced postsynaptic AP firing (output) at high frequencies in the Kv3.3KO. In vivo this manifests as reduced temporal fidelity and firing rates in the binaural auditory circuit in response to sound, whilst spontaneous AP firing increased in the Kv3.3KO. We conclude that presynaptic Kv3 channels require one (or more) Kv3.3 subunits to achieve presynaptic targeting for fast and temporally precise transmitter release at this excitatory synapse.

On deletion of Kv3.3, synaptic transmission at the calyx of Held showed accelerated recovery from short-term depression, along with increased presynaptic AP duration and increased transmitter release from WT mice of a similar age. The magnitude and fast kinetics of Kv3 channels guarantee fast repolarisation and generate a fast afterhyperpolarisation (*Brew and Forsythe, 1995*; *Figure 1B*, here) which in concert with a resurgent Na$^+$ current (*Kim et al., 2010*; *Lewis and Raman, 2014*) maximizes the availability of voltage-gated Na$^+$ channels to maintain short APs during sustained firing, as also observed in vivo (*Sierksma and Borst, 2017*). Our results on transmitter release are consistent with enhanced activity-dependent vesicle recycling in the absence of Kv3.3, as a consequence of the increased AP duration and calcium influx (*Neher and Sakaba, 2008*; *Yang et al., 2014*; *Lipstein et al., 2021*). Our modelling indicates that the increase in transmitter release is primarily an increase in vesicle release probability (and subsequent short-term depression) but an acceleration of vesicle recycling also contributes.

Changes in auditory processing over development

A key design element of this study was that each experiment compared mice of similar age against the three genotypes (WT, Kv3.3KO, and Kv3.1KO) all of which were on the same CBA background strain. Thus, variance contributed by the developmental stage was minimized within each experiment and the significant changes therefore related to the absence or presence of the Kv3 subunits under study. The range of animal ages used in this study (in different experiments) shows that Kv3.3 is relevant across development. Nevertheless, auditory responses are maturing, particularly around the onset of acoustically evoked activity (P12) in the mouse. The calyx of Held undergoes a range of developmental changes that foster temporally accurate transmission (*Borst and Soria van Hoeve, 2012*). Presynaptic calcium channels shift from N to P/Q type (*Iwasaki et al., 2000*), myelination induces developmental and activity-dependent changes (*Kim et al., 2013*; *Sinclair et al., 2017*) and similar adaptations favouring high-frequency firing are occurring in neonatal rat pups (*Sierksma and Borst, 2017*). The AP time-course accelerates (*Taschenberger and von Gersdorff, 2000*) with increased expression of Nav1.6 (*Leão et al., 2005*) which in turn influences activation of the voltage-gated calcium channels (*Borst and Sakmann, 1998*) and hence the efficacy of transmitter release (*Yang and Wang, 2006*). Presynaptic Kv currents also increase (*Nakamura and Takahashi, 2007*) with the major change being before hearing onset (and little change from P13 to P20). At the post-synaptic membrane, a concurrent switch to fast time-course GluA4-flop dominated AMPAR-mediated EPSCs (*Barnes-Davies and Forsythe, 1995*; *Geiger et al., 1995*; *Yang et al., 2011*) with developmental refinement in GluA2, reducing calcium permeability (*Lujan et al., 2019*) and a decrease in AMPAR desensitisation, further enhance transmission fidelity (*Taschenberger et al., 2002*; *Wong et al., 2003*). The present study interrogates the role of Kv3 subunits over a wide age range, from a relatively immature calyx (P10-P12) to mature adult (6 months old) and despite the inevitable developmental changes during this period, Kv3.3 remains crucial in shaping the presynaptic AP waveform and neurotransmitter release at the calyx. An increase in Kv3 expression with age may actually amplify the deficits observed in Kv3.3KOs at later developmental stages however this study shows that even with a small deficiency in Kv3.3 expression in young Kv3.3KO animals, there are drastic consequences at the synapse.

Kv3 channel subunit composition

Knowledge of Kv channel subunit composition, interactions and precise location within identified neurons is key to understanding their extensive physiological roles in controlling neuronal excitability (*Trimmer, 2015*). Kv channel building is regulated by the N-terminal tetramerisation domain (T1) (*Li et al., 1992*) to favour assembly of 'dimers of dimers' (*Tu and Deutsch, 1999*) usually from subunits within the same Kv family. Although early studies suggested otherwise, Kv3 subunits do not co-assemble with the accessory subunit gene families (Kv5, Kv6, Kv8, and Kv9) (*Bocksteins et al., 2014*), so Kv3 channels are likely composed of four Kv3 alpha subunits. Frequent co-expression of Kv3

subunits in the same neurons suggest functional channels could exist as heteromers, indeed coimmunoprecipitation has revealed interactions of Kv3.1b with Kv3.4a and Kv3.2 in globus pallidus neurons (**Baranauskas et al., 2003**; **Hernández-Pineda et al., 1999**), and with Kv3.3 in the cerebellum (**Chang et al., 2007**) but homomeric assemblies of Kv3.3 subunits could also form presynaptic Kv3 channels. The data reported here suggests that presynaptic Kv3 channels at the calyx of Held require an obligatory Kv3.3 subunit, since TEA (which will block all Kv3 heteromers) showed little effect on transmission in the Kv3.3KO. This result also implies that Kv3.1 does not have a directive or independent role in the terminal and while heteromers with Kv3.3 may occur, Kv3.1 is certainly not required for Kv3.3 localisation to the presynaptic membrane.

Could other Kv3 subunits contribute to presynaptic Kv3 channels here at the calyx or at other synapses?

Excitatory synaptic boutons, including hippocampal mossy fiber terminals (**Alle et al., 2011**), cerebellar mossy fiber terminals (**Ritzau-Jost et al., 2014**) and small neocortical boutons (**Ritzau-Jost et al., 2021**) show pharmacological evidence for presynaptic Kv3. Inhibitory interneurons also possess presynaptic Kv3 channels, including cerebellar basket cell terminals (**Southan and Robertson, 2000**) and stellate cell axons (**Rowan et al., 2016**), with the latter being identified as Kv3.4. However, it is difficult to exclude a role for Kv3.3 at this site since the Kv3 antagonist BDS is not specific for Kv3.4, having similar actions on Kv3.1 and Kv3.2; and should also block Kv3.3 subunits on the basis of sequence homology in the putative BDS binding site (**Yeung et al., 2005**). It seems unlikely that Kv3.4 (or Kv3.2) subunits have a directive (or independent) role in trafficking Kv3 channels to the calyx terminal, since the mRNA levels for these subunits was very low in the MNTB and VCN. However, if there were effective translation and assembly of Kv3.4 (or Kv3.2) into calyx Kv3 channels, then TEA should have enhanced transmitter release in the Kv3.3KO, but TEA potentiation of transmission was occluded in the Kv3.3KO.

In contrast to Kv3.1 and Kv3.2, early studies of recombinant Kv3.3 showed N-type (ball-peptide) inactivation, as originally described for Kv1 potassium channels (**Hoshi et al., 1990**). We conclude here that Kv3.3 is a principal component of presynaptic Kv3 channels but we observe little or no inactivation of the presynaptic Kv3 current. There are multiple explanations for this lack of inactivation. The degree of Kv3 inactivation varies between different expression systems (**Rudy et al., 1999**), perhaps due to there being two methionine start codons. Mammals lack a well-defined Kozak consensus sequence for the first, favouring initiation at the second methionine, thereby excluding the N-terminal peptide (**Fernandez et al., 2003**). Alternatively, endogenous PKC phosphorylation of N-terminal Kv3.3 could occlude the N-type inactivation (**Desai et al., 2008**). Also, little or no inactivation was observed in the postsynaptic Kv3.3 channel (**Choudhury et al., 2020**). Given this lack of inactivating current observed at the calyx, it is unlikely that Kv3.4 subunits are present in this terminal. Further to this, in recombinant co-expression studies, Kv3.3 and Kv3.4 did not readily form heteromers, but instead formed distinct currents with differing kinetics in the same cells (Richardson, Forsythe and Pilati, unpublished observations) suggesting that heteromeric channels composed of these subunits are unlikely.

In terminals that exhibit inactivation of presynaptic potassium currents, this has important physiological implications for transmitter release, especially during sustained high-frequency AP firing. Repetitive activation during AP trains would cause cumulative Kv3 inactivation and progressively slows AP repolarisation. This can generate a form of activity-dependent short-term potentiation where increasing AP duration potentiates transmitter release, as occurs at mossy fiber terminals (**Geiger and Jonas, 2000**). During sustained high-frequency AP firing at the calyx, the longer AP duration induced by an inactivating Kv3 would risk earlier transmission failure, with faster depletion of vesicles and inactivation of the presynaptic sodium channels. The physiological end-point for an inactivating Kv3 would be similar to that measured for the Kv3.3KO. Hence, the minimal inactivation of the presynaptic Kv3 current at the calyx of Held enables transmission to be sustained for longer, at higher firing rates and greater accuracy.

Do interactions with the cytoskeleton dictate Kv3 localisation or function?

Proximity of K^+ channels have powerful influences on the local voltage and therefore in control of other voltage-gated ion channels. The data reported here demonstrates an ionic role for Kv3.3 in

the presynaptic terminal but stabilisation in any compartment will require non-ionic interactions with components of the cytoskeleton. The permutations and complexity of channel subunit assembly optimize function through subunit-specific localisation (*Trimmer, 2015*) involving trafficking, insertion, phosphorylation, and stabilisation of channel complexes. Indeed, a general scaffolding interaction is essential for intrinsic plasticity where insertion into key sites of excitability (axon initial segments, nodes of Ranvier, heminodes and synaptic terminals) will control hyper-excitability (*Steinert et al., 2011*) and calcium overload. There is a well-established role for ankyrin-G in axonal targeting of Kv3.1b (*Xu et al., 2007*) and for clustering of sodium and potassium channels at the initial segment (*Pan et al., 2006*). Ankyrin-R binds and stabilizes Kv3.1b in fast spiking interneuron somatic membranes and nodes of Ranvier; and crosslinks Kv3.3 via spectrin to the cytoskeleton in Purkinje neurons, which aids their survival (*Stevens et al., 2021*; *Stevens et al., 2022*). This interaction of both subunits with ankyrin-R would explain the inability of the MNTB neuron soma to differentiate or partition channels composed of Kv3.1b or Kv3.3 subunits (*Choudhury et al., 2020*) so that each subunit type could largely compensate for the absence of the other within the soma. Presynaptic stabilisation of Kv3.3 however, is unlikely to be through ankyrin-R alone, as this mechanism would not discriminate between the subunits.

Another possibility is that Kv3.3 inactivation is suppressed by the C-terminus associating with Hax1 (*Blosa et al., 2015*) to bind the Kv3.3 N-Terminal ball peptide and modulate the actin network. However, as in the WT, the calyceal outward currents reported in *Zhang et al., 2016* were an order of magnitude smaller than observed here or elsewhere. Additionally, the presynaptic K$^+$ currents from a Kv3.3KO calyx were similar magnitude to WT (Figure S4: *Zhang et al., 2016*). Based on association with the actin cytoskeleton, deletion of Kv3.3 was proposed to inhibit endocytosis in the calyx synaptic terminal by this non-ionic mechanism (*Wu et al., 2021*). However, the *Wu et al., 2021* study does not test for the possibility of a simultaneous ionic mechanism or for a change in the presynaptic AP waveform on deletion or mutation of Kv3.3. With the evidence reported here, it is clear that Kv3.3 does have an ionic role at the calyx of Held. Our observations on EPSCs and modelling of short-term depression show that Kv3.3 deletion increases transmitter release and accelerates a fast sub-second component of activity-dependent recycling (*Figure 5F*, inset) following conditioning stimulation. Although this contrasts with the slowing of endocytosis observed in *Wu et al., 2021* our observations are over a much shorter time-course and measure EPSC amplitude, rather than presynaptic capacitance. Future experiments will determine what part of the endocytosis capacitive changes result from direct or indirect ionic mechanisms versus non-ionic mechanisms.

Relevance of Kv3.3 to mechanisms of sound localisation

The kinetics of Kv3 channels is fast enough to generate a rapid afterhyperpolarisation following the AP, which maximises the driving force for calcium influx and promotes recovery of voltage-gated sodium and calcium channels from inactivation. Short duration APs permit high firing rates by minimising the absolute refractory period, thus Kv3 enables well-timed high-frequency AP trains and when input firing rates exceed the refractory limit, neurons expressing Kv3 readily switch to firing on alternate input spikes (*Song et al., 2005*). In this study, we evoked MNTB neuron AP firing in response to presynaptic stimulation and asked how effective was the input/output relationship across a range of firing frequencies from 100 to 600 Hz in each genotype. Although there was little difference at low firing frequencies, at the highest frequencies only the first few presynaptic APs generate postsynaptic APs with 1:1 fidelity (Phase I) before entering a chaotic phase (Phase II) with many failures, which resolves later in the train into precise firing but to alternate stimuli (Phase III). In the absence of Kv3.3 the MNTB firing passed into Phase II but did not converge into Phase III firing, consistent with the idea that presynaptic Kv3.3 improved stability of synaptic transmission.

Integration of information from both ears for the purpose of sound localisation requires high temporal accuracy for bilateral transmission of auditory APs from each cochlea to the superior olivary complex (*Tollin, 2003*; *Joris and Trussell, 2018*). This is facilitated by Kv3 channels within specific neurons, from cell bodies, axons, synaptic terminals and across the neural network. In vivo extracellular recording from the MNTB measures simultaneously the presynaptic calyx and postsynaptic MNTB single unit APs. Accurate transmission of AP timing was compromised in the Kv3.3KO, and the peak firing rate was reduced. Additionally, spontaneous AP firing was elevated (with respect to WT animals), likely reflecting hyper-excitability upstream in the auditory pathway, with Kv3.3 being

expressed in spiral ganglion (*Kim et al., 2020*) and the globular bushy cells (*Li et al., 2001*; *Cao et al., 2007*) which give rise to the calyx of Held. The use of anesthetic for our in vivo study may affect auditory processing, but comparison with multiple other studies in mice and gerbil and using a range of different anesthetics showed that the synaptic delay measured in this study was favourably comparable to these other studies: ketamine/xylazine in mouse: 0.40ms (*Blosa et al., 2015*), 0.46ms (*Kopp-Scheinpflug et al., 2003*), 0.50ms (*Lorteije et al., 2009*) ketamine/xylazine in gerbil: 0.44ms (*Tolnai et al., 2009*). This narrow distribution of synaptic delays with different anesthesia suggests that the effect of anesthesia on synaptic delay is negligible compared to the effect of deleting Kv3.3.

Kv3.3 physiology, dysfunction, and disease

Immunohistochemical studies have localized Kv3.3 subunits to many different synaptic terminals across the brain, from spiral ganglion afferent processes (*Kim et al., 2020*), medial vestibular nuclei (*Brooke et al., 2010*), cerebellar dentate nucleus (*Alonso-Espinaco et al., 2008*), parallel fiber synapses (*Puente et al., 2010*), posterior thalamic nucleus (*Chang et al., 2007*), and the neuromuscular junction (*Brooke et al., 2004*). It is interesting to consider why Kv3.3 is present at some synaptic terminals, but not all. One hypothesis is that presynaptic Kv3.3 would enhance resource and energy conservation during high frequency firing, but more importantly it will support the physiological mechanisms as a synapse evolves from a microdomain to a nanodomain architecture for exocytosis (*Meinrenken et al., 2003*; *Young and Veeraraghavan, 2021*) by constraining presynaptic calcium influx.

Disease mutations associated with Kv3.3, such as spinocerebellar ataxia type 13 (SCA13) cause multiple neurological defects, which from the evidence reported here could include aberrant neurotransmitter release in addition to postsynaptic excitability changes. In the case of the SCA13 mutation R420H (*Middlebrooks et al., 2013*), the observations made here support the hypothesis that SCA13 disrupts the physiological process of interaural level discrimination by reducing the gain and signal to noise ratio, thereby undermining sound source localisation (*Tollin, 2003*). The current study suggests several areas for further investigation of presynaptic potassium conductances: First, the contribution of ionic and non-ionic mechanisms is now recognized for Kv3 and their relative contribution to cytoskeleton and physiology can be elucidated. Second, it is necessary to determine which spliced-variants or potassium channel beta subunits/accessory proteins are expressed and how subunit phosphorylation contributes to the physiology. Third, while Kv3.3 can be clearly resolved on the non-release face of the terminal, the resolution on the release face is not sufficient to unambiguously distinguish between the pre- and post-synaptic membranes, but in order to avoid depolarisation by $[K^+]_o$ accumulation, one would predict minimal potassium efflux into the synaptic cleft. Fourth, Kv3 currents do not mediate all the presynaptic potassium current and other Kvs operating at more negative voltage activation ranges, such as Kv1 (*Geiger and Jonas, 2000*; *Dodson et al., 2003*) or Kv7 (*Zhang et al., 2022*) are likely to contribute to terminal threshold, excitability and AP waveform.

The combinatorial potential of Kv3 channel subunits gives rise to a spectrum of physiological roles in fast-spiking neurons (*Choudhury et al., 2020*) and interneurons (*Chang et al., 2007*). The pre- and postsynaptic studies conducted here at the calyx of Held/MNTB neuron clearly show that Kv3.3 subunits are critical for presynaptic localisation of Kv3 channels mediating fast AP repolarisation. They contribute to improved temporal accuracy and conservation of presynaptic resources during high-frequency firing. Together these results suggest a general role for Kv3.3 in raising the biophysical 'speed limit' for information transmission at fast synapses, especially during intense synaptic activity.

Materials and methods

Key resources table

Reagent type (species) or resource	Designation	Source or reference	Identifiers	Additional information
Genetic reagent (*M. musculus*)	CBA/Crl	Charles River	Strain code: 609	Leicester breeding colony

Continued on next page

Continued

Reagent type (species) or resource	Designation	Source or reference	Identifiers	Additional information
Genetic reagent (*M. musculus*)	Kv3.1 knockout mouse on CBA back-ground (Kv3.1KO)	Ho et al, PNAS 94, 1533–1,538. 1997.	CBA/CaCrl.*Kcnc1*tm1Joho/UoL	Strain originally created on 129/SV background and backcrossed onto CBA for >10 generations at the Preclinical Research Facility – University of Leicester
Genetic reagent (*M. musculus*)	Kv3.3 knockout mouse on CBA back-ground (Kv3.3KO)	Espinosa et al., J Neurosci 21, 6657–6,665. 2001	CBA/CaCrl. *Kcnc3*tm1Echa/UoL	Strain was originally created on C57BL/6 background and backcrossed onto CBA for >10 generations at the Preclinical Research Facility – University of Leicester
Commercial assay or kit	Illumina NextSeq500 High Output	Illumina	FC-404–2002	Used for Cochlear Nucleus
Chemical compound, drug	Strychnine hydrochloride	Sigma Aldrich (MERCK)	S8753-25G	(0.5 μM)
Chemical compound, drug	Tetraethylammonium	Sigma Aldrich (MERCK)	86614–25 G	(1 mM)
Chemical compound, drug	Fentanyl	Janssen	6,001	(0.05 mg/kg)
Chemical compound, drug	Midazolam	B Braun	17206034	(5.0 mg/kg)
Chemical compound, drug	Medetomidine	Vetoquil GmbH	Domitor	(0.5 mg/kg)
Antibody	Anti-Kv3.1b (rabbit polyclonal)	Alomone	APC-014	(1:1000)
Antibody	Anti-Kv3.3 (mouse monoclonal)	Neuromab	75–354	(1:3000)
Antibody	Alexafluor488 Goat anti-rabbit (Goat polyclonal)	Thermofisher	A-11008	(1:1000)
Antibody	Alexafluor546 Goat anti-mouse (Goat polyclonal)	Thermofisher	A-11003	(1:1000)
Antibody	Anti-Kv3.1b (rabbit polyclonal)	Synaptic systems	242 003 (Lot# 1–2)	(1:300)
Antibody	Anti-Kv3.3 (rabbit polyclonal)	Alomone	APC-102 (Lot# APC 102AN0502)	(1:300)
Antibody	Anti-Bassoon (mouse monoclonal)	Synaptic systems	141 111 (Lot# 1–2)	(1:300)
Antibody	Alexafluor488 Goat anti-mouse (goat polyclonal)	Invitrogen	A11001 (Lot# 21 40660)	(1:300)
Antibody	Alexafluor546 Goat anti-rabbit (goat polyclonal)	Invitrogen	A11010 (Lot# 21 89179)	(1:300)
Software, algorithm	Graphpad Prism 9.0.2	Graphpad	RRID:SCR _002798	
Software, algorithm	pClamp 10 software suite	Molecular Devices	RRID:SCR _011323	
Software, algorithm	Zen Blue, 3.1	Zeiss	RRID:SCR _013672	
Software, algorithm	ABR Averager (Custom)	Wellcome Trust Sanger Institute		
Software, algorithm	AudioSpike	HoerrTech	https://audiospike.hz-ol.de/	
Software, algorithm	MATLAB R2010a	Mathworks	RRID:SCR_001622	

Continued on next page

Continued

Reagent type (species) or resource	Designation	Source or reference	Identifiers	Additional information
Software, algorithm	Fiji	NIH ImageJ	RRID:SCR_002285	
Other	Custom concentric bipolar stimulating electrodes	FHC	CBASD75	
Other	Borosilicate glass capillaries	WPI	GC150F-7.5	

Experiments were conducted in accordance with the Animals (Scientific Procedures) Act UK 1986 and as revised by the European Directive 2010/63/EU on the protection of animals used for scientific purposes. All procedures were approved by national oversight bodies (UK Home Office, or Bavarian district government, ROB-55.2–2532.Vet_02-18-1183) and the local animal research ethics review committees.

Experiments were conducted on CBA/Crl mice (wildtype, WT) and knockouts were backcrossed for 10 generations onto this CBA/Crl background (*Choudhury et al., 2020*). PCR genotyping was done from ear notch samples made at P10. Mice were housed and breeding colonies maintained at the preclinical research facility (PRF) at the University of Leicester, subject to a normal 12 hr light/dark cycle and with free access to food and water (ad libitum). Both male and female animals were used in experiments with ages ranging from P10-25 for electrophysiology to 6 months of age for in vivo and auditory brainstem response (ABR) recordings.

mRNA sequencing

Mice were killed by decapitation and brainstems were removed into 'RNA Later' stabilisation solution (Invitrogen, Cat# AM7020), before dissection to isolate both cochlear nuclei. Tissue from 3 CBA/Crl mice were pooled into 9 individual samples (27 mice total) before phenol extraction to isolate RNA. RNA purity, integrity, and concentration was assessed by UV-Vis spectroscopy (Nanodrop 8000) and capillary electrophoresis (Agilent Bioanalyzer 2000). Samples with RIN (RNA integrity)<7 were discarded. cDNA libraries were constructed using the NEBNext Ultra Directional RNA Library Prep Kit for Illumina sequencing performed using the Illumina NextSeq500 High Output (v2, 150 cycles) kit and the Illumina NextSeq500. Analysis of sequencing data was performed using Illumina Basespace. Using FastQC toolkit (Babraham Bioinformatics) total reads were trimmed of low-quality reads (Q<20), poly-A/T tails >10 bp, and adapter sequences before alignment to the mm10 (GRCM387) mouse genome (Ensembl) using TopHat2. Output values represented as Fragments per kilobase of transcript per million mapped reads (FPKM).

Electrophysiology

In vitro brain slice preparation

Mice were killed by decapitation, the brainstem removed and placed into ice-cold artificial cerebro-spinal fluid aCSF, oxygenated with 95%O_2/5%CO_2, containing (in mM): sucrose (250), KCl (2.5), NaHCO₃ (26), NaH₂PO₄ (1.25), D-Glucose (10), ascorbic acid (0.5) MgCl₂ (4), and CaCl₂ (0.1). For presynaptic recordings, 100-μm-thick transverse slices or 250-μm-thick slices for postsynaptic recordings were prepared in a pre-cooled chamber using a Leica VT1200S vibratome. Slices were allowed to recover for 1 hr at 37 °C in normal aCSF (*Choudhury et al., 2020*), continually bubbled with 95%O_2/5%CO_2 and subsequently allowed to passively cool to room temperature. The aCSF (310 mOsm) contained (in mM): NaCl (125), NaHCO₃ (26), D-Glucose (10), KCl (2.5), myo-inositol (3), NaH₂PO₄ (1.25), sodium pyruvate (1), ascorbic acid (0.5), MgCl₂ (1), and CaCl₂ (2). Recordings from brain slices were conducted at a temperature of 35±1°C.

Presynaptic recordings

Mice aged P10-P12 were used for presynaptic calyx recordings. For each experiment, slices were placed in a recording chamber of a Nikon E600FN upright microscope and cells visualized with a 60 x DIC water-immersion objective (*Lucas et al., 2018*). Slices were continuously perfused with normal aCSF saturated with 95%O_2/5%CO_2, (as above), heated to 35 °C±1, at a rate of 1 ml/min. Whole-cell patch recordings were made using thick-walled borosilicate capillaries (1.5 mm OD, 0.86 mm ID) with

a resistance of 4–6 MΩ, filled with an internal solution composed of (in mM): KGluconate (97.5), KCl (32.5), HEPES (40), EGTA (0.2), MgCl$_2$ (1), K$_2$ATP (2.2), Na$_2$GTP (0.3), pH adjusted to 7.2 with KOH (295 mOsm). Calyces were identified visually, appearing as a second membrane profile around an MNTB principal neuron (*Billups and Forsythe, 2002a*; *Billups et al., 2002b*) using Differential Interference Contrast (DIC) optics. Presynaptic recordings were confirmed here through the total absence of spontaneous miniature synaptic events. (In 40 terminals 0 miniature synaptic events were observed in each 16 s calyceal recording (n=40) vs 10±7 events per second when recording from MNTB principal neuron; n=9, mice aged P10-P12). If any single spontaneous synaptic event was observed in a presynaptic recording, this data set was excluded. Additional criteria for calyceal recordings were that APs had a pronounced depolarising after-depolarisation potential (DAP, *Borst et al., 1995*; *Dodson et al., 2003*; *Kim et al., 2010*), a high membrane input resistance, a fast I$_H$ current (*Cuttle et al., 2001*) as opposed to a slow I$_H$ in the postsynaptic MNTB neuron (*Kopp-Scheinpflug et al., 2015*) and a resting membrane potential of around –70 mV, compared to –60 mV for postsynaptic neurons.

Recordings were made with a Multiclamp 700A amplifier (Molecular Devices), 1322A digidata (Axon Instruments) and pClamp 10 software (Molecular Devices) for acquisition and analysis. Electrode and cell capacitance were compensated and series resistances were corrected, with recordings discarded when series resistances reached >20 MΩ before compensation. All recordings were compensated by 70%. Signals were digitized at 100 kHz and filtered at 10 kHz. The stated voltages were not corrected for a liquid junction potential of 11 mV.

Current-voltage relationships were generated in voltage-clamp over a range of command voltages from –110 mV to +30 mV in 10 mV incremental steps. Steps were 150 ms in duration and separated by 1 s intervals. Action potentials measured in current-clamp were generated using short depolarising current steps (50 pA increments) of 50 ms duration, the first (threshold) evoked action potential was analyzed. Pipette capacitance was neutralized and the bridge balanced. Hyperpolarising current steps (–50 pA, 150 ms) were used to determine membrane resistance. For both voltage and current clamp experiments, voltage or current commands were from –70 mV.

Postsynaptic recordings

The same experimental setup as described above was used for postsynaptic recordings. Borosilicate glass pipettes (2.5–3.5 MΩ resistance) were filled with a solution containing (in mM) KGluconate (120), KCl (10), HEPES (40), EGTA (0.2), MgCl$_2$ (1), K$_2$ATP (2.2). Electrode and cell capacitance were compensated and series resistances were corrected, with recordings discarded when series resistances reached >10 MΩ (before compensation) or changed by >10% during the recording. All recordings were compensated by 70%, signals were digitized at 100 kHz and filtered at 10 kHz.

Mice aged P20-P27 were used for studying synaptic physiology. Axons giving rise to the calyx terminal were stimulated using a concentric bipolar electrode (FHC, inc #CBAD75S) placed at the midline of a brainstem slice, controlled by a constant voltage stimulator box (DS2A, Digitimer) triggered by the pClamp 10 software. Axons were subjected to low-frequency stimulation (0.3 Hz) in order to determine the threshold for generating evoked excitatory postsynaptic currents (EPSCs) after which stimulation trains of 5 × 100, (separated by 20 s intervals), 200 and 600 Hz for 800ms separated by 30 s intervals were applied. Time was allowed for the internal patch solution to equilibrate (5 min) before stimulation trains were applied. EPSC recordings were conducted from a holding potential of –40 mV (to inactivate voltage-gated sodium channels) and inhibitory transmission blocked by adding 0.5 µM strychnine hydrochloride to external aCSF.

Postsynaptic recordings of action potential trains at high frequencies

Current clamp recordings were made from MNTB neurons stimulated presynaptically with a bipolar concentric electrode (FHC, inc #CBAD75S). Trains of 0.1 ms stimuli of variable voltages (3–15 V) were delivered to the presynaptic axon at 100, 200, 300, 400, and 600 Hz using a constant voltage stimulation box (DS2A, Digitimer) triggered by the pClamp10 software. Evoked responses were recorded from the postsynaptic neuron under current clamp, with resting membrane potentials adjusted to –60 mV. Stimulation trains of the duration of 800 ms at the different frequencies were repeated 3 times and separated by 20 s intervals to allow for recovery.

Voltage and current-clamp analysis

Electrophysiology analysis was conducted using Clampfit 10 software (Molecular Devices). Current amplitudes were measured as the steady-state current towards the end of the 150 ms voltage step. Presynaptic action potentials were analyzed using the threshold detection function. The threshold was set to the voltage of action potential activation and the relative amplitude defined as the difference between voltage at the peak and voltage at the threshold. Half-width is defined as the time delay between upstroke and downstroke at half-maximal amplitude. Rise and decay slopes were measured from 10% to 90% of peak amplitude.

Single excitatory postsynaptic currents were analyzed using the threshold detection function in pClamp. Baseline was defined as the resting current before stimulation. The threshold for detection was set to twice the standard deviation of the noise level. Peak amplitudes were defined as the difference between the current at the peak and the current at the baseline. Rise times were measured from 10% to 90% of the peak and decay taus were measured by fitting an exponential curve on the decay phase from 90% of the peak value. Charge was measured as the area under the curve, between the peak and baseline.

EPSC trains were analyzed by normalising each response to the first response in the train then fitting a single exponential to normalized amplitudes of responses and extracting the decay tau and steady-state amplitudes of the exponential fit to define the rate at which responses underwent short-term depression and the extent to which they depressed. mEPSCs were analyzed using template detection. A template of mEPSC kinetics was created by manually selecting 20 mEPSCs. This was then used for automatic detection of mEPSCs in all files.

Immunofluorescence

Immunohistochemistry was conducted using similar methods to those reported in *Choudhury et al., 2020*. Briefly, mice aged 28 days were killed by decapitation and the brainstem dissected and immediately snap frozen in OCT before cutting at 12 μm transverse slices on a cryostat. Sections were mounted on poly-L-Lysine (Sigma Aldrich P8920) coated glass slides. For brainstem sections, tissues were removed and post-fixed with 4% PFA for 10 min at 4 °C. Antigen retrieval was achieved by incubating fixed tissues in a 10 mM Citrate buffer for 20 min at 85–90°C. For the cochlea both inner ears were dissected and fixed by perfusion at the round and oval window with 4% PFA in 1xPBS + 0.1% TritonX-100 (PBST), followed by overnight submersion in fixative at 4 °C. Cochlea sections were cut from whole tissues decalcified for 72 hr at 4 °C in 4% EDTA, cryoprotected with 30% sucrose, then embedded in OCT before sectioning at 12 μm on a cryostat and mounted on poly-L-Lysine (Sigma Aldrich P8920) glass slides. Antigen retrieval was achieved by 5 min incubation in 1% SDS prior to staining. Low-affinity binding was blocked using 10% Normal Goat Serum +1% BSA in PBST ('blocking solution') for 1 hr at room temperature. Afterwards primary antibodies for Kv3.1b (Rabbit, Alomone APC-014, 1:1000) and Kv3.3 (Mouse, Neuromab 75–354, 1:3000) were diluted in blocking solution and incubated overnight at 4 °C. Following 3 × 10 min washes in PBST, sections were incubated for 2 hours at room temperature with the appropriate secondary antibodies diluted 1:1000 in blocking solution (AF488 Goat Anti-Rabbit, A-11008; AF546, Goat Anti-Mouse, A-11003, Thermo Fisher). Slides were washed 3 × 20 min in PBST before cover slipping with hard-set mounting medium (Vectashield, H-1400) and stored at 4 °C. Slides were imaged using Leica DM 2500 and image analysis performed using Fiji software. The same observations were made in at least 3 animals for WT and 2 animals for each KOs.

Protein retention expansion microscopy (proExM)

Mice aged P28-P30 were killed by decapitation, their brain dissected and brainstem sectioned to obtain transverse slices of 100 μm thickness. Tissue from three animals per genotype was used for each investigation. Free-floating brain slices underwent fixation (PBST, 4% PFA, 4 °C, 15 min), and then washed in PBST (3 × 10 min). A tissue blocking stage (RT, 1 h) was used to minimize low affinity binding with 1% BSA +10% Normal Goat Serum (Vector Laboratories S-1000) in PBST ('blocking solution'). Free floating slices were incubated with the primary antibodies in a petri dish: Anti-Kv3.1b rabbit (Synaptic Systems 242 003 Lot# 1–2, polyclonal), or Anti-Kv3.3 rabbit (Alomone APC-102 Lot# APC102AN0502, polyclonal), and Bassoon mouse Cl179H11 (Synaptic Systems 141 111 Lot# 1–2, monoclonal), diluted in blocking solution (1:300 for all primary Abs) and incubated overnight at room

temperature on a shaker. The slices were washed 3 × 10 min in PBST, and incubated with the respective secondary antibodies (AF488 goat anti-mouse IgG, 1:300 Invitrogen A11001, Lot# 2140660; AF546 goat anti-rabbit IgG, 1:300 Invitrogen A11010, Lot# 2189179) for 2 hr at room temperature on a shaker. Slices were washed 3 × 10 min in PBST and incubated with 0.1 mg/ml 6-((acryloyl)amino) hexanoic acid (AcX) solution in PBS overnight with no shaking, followed by 2 × 15 min wash in PBS. The slices were then 'gelled' and the gels digested according to the proExM protocol for intact tissues (basic protocol 2, *Asano et al., 2018*). The digested gels were expanded in ddH$_2$O water for 3 × 20 min for same-day imaging or stored at 4 °C in the dark in PBS for later use. For imaging, gels were transferred to 35 mm glass-bottom petri dishes with a sealed lid, previously coated with poly-L-Lysine (Sigma Aldrich P8920). Fluorescence imaging was conducted using a Zeiss LSM 980 Airyscan 2 microscope and images were processed using ZEN 3.1 (blue edition) and Fiji software. Controls for non-specific immunostaining of the secondary antibodies (incubations without the primary antibody, data not shown), and pre-incubation of each primary antibody with the corresponding antigenic peptide (blocking peptide) were conducted as part of the antibody validation procedure. Immunostaining with Kv3.1b and Kv3.3 primary antibodies was confirmed as absent in the corresponding knockout tissues.

In vivo physiology
Adult (6–8 month) Kv3.3 knockout mice of either sex (n=5) and five age-matched CBA wild type mice were anesthetized with a subcutaneous injection of 0.01 ml/g MMF (0.5 mg/kg body weight Medetomidine, 5.0 mg/kg body weight Midazolam and 0.05 mg/kg body weight Fentanyl). They were placed on a temperature-controlled heating pad (WPI: ATC 1000) in a soundproof chamber (Industrial Acoustics). Depth of anesthesia was measured using the toe pinch reflex and animals responding were given supplemental MMF at 1/3 the initial dose. The mice were stabilized in a custom stereotaxic device. An incision was made at the top of the skull, followed by a craniotomy just anterior to the lambda suture intersection. The skull was tilted to provide access to the auditory brainstem. A ground electrode was placed in the muscle at the base of the neck. Glass microelectrodes were pulled from glass capillaries so that the resistance was 5–20 MΩ when filled with 3 M KCl solution. Signals were amplified (AM Systems, Neuroprobe 1600), filtered (300–3000 Hz; Tucker-Davis-Technologies PC1) and recorded (~50 kHz sampling rate) with a Fireface UFX audio interface (RME). AudioSpike software (HoerrTech) was used to calibrate the multi-field magnetic speakers, generate stimuli and record action potentials. Stimuli consisted of pure tones (50–100 ms duration, 5ms rise/fall time) at varying intensity (0–90 dB SPL) and were presented through hollow ear bars connected to the speakers with Tygon tubing. PSTHs were assessed at characteristic frequency (CF) and 80 dB SPL. MNTB neurons were identified by their excitatory response to contralateral sound stimulation and their typical complex waveform (*Kopp-Scheinpflug et al., 2003*), consisting of a presynaptic potential (preAP), a synaptic delay (SD) and a postsynaptic potential (AP).

Auditory-evoked brainstem response
ABR equipment set-up and recordings have previously been described in detail in *Ingham et al., 2011*. Briefly, mice were anesthetized with fentanyl (0.04 mg/kg), midazolam (4 mg/kg), and medetomidine (0.4 mg/kg) by intraperitoneal injection. Animals were placed on a heated mat inside a sound-attenuated chamber, and electrodes were inserted sub-dermally; below the right pinnae, into the muscle mass below the left ear, and at the cranial vertex. ABR responses were collected, amplified, and averaged using the TDT System3 (Tucker Davies Technology) in conjunction with custom 'Averager' software, provided by the Wellcome Trust Sanger Institute. Binaural stimuli were delivered in the form of a 0.1ms broadband click. All stimuli were presented in 5 dB SPL rising steps to 95 dB SPL, and responses were averaged 512 times per step. Recordings were averaged over a 20ms period with a 300–3000 Hz bandwidth filter and a gain of 25,000 x. Wave amplitude and latencies were analyzed using the Auditory Wave Analysis Python script developed by Bradley Buran (Eaton-Peabody Laboratory), and calculated as the difference between peak and valley (μV) and time to wave peak (s), respectively.

Computation model
A simple model with activity-dependent vesicle recycling (*Graham et al., 2004*; *Billups et al., 2005*; *Lucas et al., 2018*) was used. In the model, vesicles in a releasable pool of normalized size *n* may

release with a fixed probability $P=P_v$ on the arrival of a presynaptic action potential at time s to give an EPSC amplitude proportional to np (equ. 3). Vesicles in this releasable pool are replenished up to the maximum normalised pool size of $n=1$ at a rate τ_r from an infinite reserve pool (equ. 1). In the absence of presynaptic action potentials, replenishment proceeds at a constant background rate (time constant τ_b). Following a presynaptic action potential, the replenishment rate is instantaneously raised to a higher rate, τ_h (equ. 2b) which then decays back to the background rate with time constant τ_d (equ. 2 a). The model equations are:

$$\frac{dn}{dt} = \frac{1-n(t)}{\tau_r(t)} - \sum_s P_v . n(t) . \delta(t-s) \tag{1}$$

$$\frac{d\tau_r}{dt} = \frac{\tau_b - \tau_r(t)}{\tau_d} \tag{2a}$$

$$\tau_r(s) = \tau_h \tag{2b}$$

$$EPSC(s) = n(s) . P_v \tag{3}$$

The model is implemented in Matlab. Differential equations are solved by simple forward Euler integration.

Statistics

Statistical analysis of the in vitro data was performed in Graphpad Prism V7 unless otherwise specified. Data were tested for a normal gaussian distribution using a Shapiro-Wilk normality test and parametric (one-way ANOVA) or non-parametric tests (Kruksal-Wallis ANOVA) applied as appropriate. Multiple comparisons were corrected for using Tukey's multiple comparisons test or Dunn's multiple comparison test post-hoc and a p value of<0.05 was taken as significant. The statistical tests applied are noted in the figure legends and corresponding text. Data is represented as mean ± SD unless otherwise stated. In vivo data are presented as medians and inter-quartiles in text numbers and figures in addition to individual data points. Statistical analyses of the in vivo data were performed with SigmaStat/SigmaPlot. Normality was tested by the Shapiro-Wilk Test. Comparisons between data sets were made using parametric tests for normally distributed data (two-tailed Student's t-test for comparing two groups) and when the normality assumption was violated, a non-parametric test (Mann-Whitney Rank Sum Test) was used.

Acknowledgements

Additional information

Competing interests

Nadia Pilati: This author is employed by Autifony Therapeutics Ltd. The other authors declare that no competing interests exist.

Author ORCIDs

Amy Richardson http://orcid.org/0000-0002-1552-2915
Victoria Ciampani http://orcid.org/0000-0002-4154-1562
Kseniia Bondarenko http://orcid.org/0000-0003-3321-9423
Sherylanne Newton http://orcid.org/0000-0002-8210-3526
Joern R Steinert http://orcid.org/0000-0003-1640-0845
Ian D Forsythe http://orcid.org/0000-0001-8216-0419

Ethics

Experiments were conducted in accordance with the Animals (Scientific Procedures) Act UK 1986 and as revised by the European Directive 2010/63/EU on the protection of animals used for scientific purposes. All procedures were approved by national oversight bodies (UK Home Office, or Bavarian district government, ROB-55.2-2532.Vet_02-18-1183) and the local animal research ethics review committees. In vivo experiments were conducted under anaesthesia: with a subcutaneous injection of 0.01ml/g MMF (0.5mg/kg body weight Medetomidine, 5.0mg/kg body weight Midazolam and 0.05mg/kg body weight Fentanyl). Every effort was made to minimise suffering and at the end of each procedure the animal was humanely killed using an approved method.

Decision letter and Author response

Decision letter https://doi.org/10.7554/eLife.75219.sa1
Author response https://doi.org/10.7554/eLife.75219.sa2

Additional files

Supplementary files

• Supplementary file 1. Summary table of averaged data and statistical tests presented in the figures, including significant (red) and non-significant values (black). Data are presented in the same order as figures appear in the article. Details are provided about the number of animals, number of cells, statistical test used and calculated p values.

• Transparent reporting form

Data availability

Data generated in this study are included in the manuscript and supporting files. Source data files for each figure has been uploaded onto FigShare. Datasets Generated for the Ms "Kv3.3 subunits control presynaptic action potential waveform and neurotransmitter release at a central excitatory synapse" Authors: Ian D. Forsythe, Amy Richardson, Victoria Ciampani, Mihai Stancu, Kseniia Bondarenko, Sherylanne Newton, Joern Steinert, Nadia Pilati, Bruce Graham, Conny Kopp-Scheinpflug, 2022, https://figshare.com/s/9c0a07ed2fe5761cc281. The model code and associated data files are available at: Bruce Graham, 2021, https://github.com/bpgraham/CoH-Models, (copy archived at swh:1:rev:6ae468a42fc94dec2cf3f7c5490593ee321c8321).

The following datasets were generated:

Author(s)	Year	Dataset title	Dataset URL	Database and Identifier
Forsythe ID, Richardson A, Ciampani V, Stancu M, Bondarenko K, Newton S, Steinert J, Pilati N, Graham B, Kopp-Scheinpflug C	2022	Kv3.3 subunits control presynaptic action potential waveform and neurotransmitter release at a central excitatory synapse	https://doi.org/10.25392/leicester.data.19322864.v1	figshare, 10.25392/leicester.data.19322864.v1
Graham B	2021	The model code and associated data files	https://github.com/bpgraham/CoH-Models	GitHub, bpgraham/CoH-Models

References

Alle H, Kubota H, Geiger JRP. 2011. Sparse but highly efficient Kv3 outpace BKCa channels in action potential repolarization at hippocampal mossy fiber boutons. *The Journal of Neuroscience* **31**:8001–8012. DOI: https://doi.org/10.1523/JNEUROSCI.0972-11.2011, PMID: 21632922

Alonso-Espinaco V, Elezgarai I, Díez-García J, Puente N, Knöpfel T, Grandes P. 2008. Subcellular localization of the voltage-gated potassium channels Kv3.1b and Kv3.3 in the cerebellar dentate nucleus of glutamic acid decarboxylase 67-green fluorescent protein transgenic mice. *Neuroscience* **155**:1059–1069. DOI: https://doi.org/10.1016/j.neuroscience.2008.07.014, PMID: 18682278

Asano SM, Gao R, Wassie AT, Tillberg PW, Chen F, Boyden ES. 2018. Expansion Microscopy: Protocols for Imaging Proteins and RNA in Cells and Tissues. *Current Protocols in Cell Biology* **80**:e56. DOI: https://doi.org/10.1002/cpcb.56, PMID: 30070431

Baranauskas G, Tkatch T, Nagata K, Yeh JZ, Surmeier DJ. 2003. Kv3.4 subunits enhance the repolarizing efficiency of Kv3.1 channels in fast-spiking neurons. *Nature Neuroscience* **6**:258–266. DOI: https://doi.org/10.1038/nn1019, PMID: 12592408

Barnes-Davies M, Forsythe ID. 1995. Pre- and postsynaptic glutamate receptors at a giant excitatory synapse in rat auditory brainstem slices. *The Journal of Physiology* **488**:387–406. DOI: https://doi.org/10.1113/jphysiol.1995.sp020974, PMID: 8568678

Beiderbeck B, Myoga MH, Müller NIC, Callan AR, Friauf E, Grothe B, Pecka M. 2018. Precisely timed inhibition facilitates action potential firing for spatial coding in the auditory brainstem. *Nature Communications* **9**:1771. DOI: https://doi.org/10.1038/s41467-018-04210-y, PMID: 29720589

Billups B, Forsythe ID. 2002a. Presynaptic mitochondrial calcium sequestration influences transmission at mammalian central synapses. *The Journal of Neuroscience* **22**:5840–5847., DOI: https://doi.org/20026597, PMID: 12122046

Billups B, Wong AYC, Forsythe ID. 2002b. Detecting synaptic connections in the medial nucleus of the trapezoid body using calcium imaging. *Pflugers Archiv* **444**:663–669. DOI: https://doi.org/10.1007/s00424-002-0861-6, PMID: 12194020

Billups B, Graham BP, Wong AYC, Forsythe ID. 2005. Unmasking group III metabotropic glutamate autoreceptor function at excitatory synapses in the rat CNS. *The Journal of Physiology* **565**:885–896. DOI: https://doi.org/10.1113/jphysiol.2005.086736, PMID: 15845577

Blosa M, Sonntag M, Jäger C, Weigel S, Seeger J, Frischknecht R, Seidenbecher CI, Matthews RT, Arendt T, Rübsamen R, Morawski M. 2015. The extracellular matrix molecule brevican is an integral component of the machinery mediating fast synaptic transmission at the calyx of Held. *The Journal of Physiology* **593**:4341–4360. DOI: https://doi.org/10.1113/JP270840, PMID: 26223835

Bocksteins E, Mayeur E, Van Tilborg A, Regnier G, Timmermans JP, Snyders DJ. 2014. The subfamily-specific interaction between Kv2.1 and Kv6.4 subunits is determined by interactions between the N- and C-termini. *PLOS ONE* **9**:e98960. DOI: https://doi.org/10.1371/journal.pone.0098960, PMID: 24901643

Borst JGG, Helmchen F, Sakmann B. 1995. Pre- and postsynaptic whole-cell recordings in the medial nucleus of the trapezoid body of the rat. *The Journal of Physiology* **489**:825–840. DOI: https://doi.org/10.1113/jphysiol.1995.sp021095, PMID: 8788946

Borst JGG, Sakmann B. 1998. Calcium current during a single action potential in a large presynaptic terminal of the rat brainstem. *The Journal of Physiology* **506**:143–157. DOI: https://doi.org/10.1111/j.1469-7793.1998.143bx.x, PMID: 9481678

Borst JGG, Soria van Hoeve J. 2012. The calyx of Held synapse: from model synapse to auditory relay. *Annual Review of Physiology* **74**:199–224. DOI: https://doi.org/10.1146/annurev-physiol-020911-153236, PMID: 22035348

Brew HM, Forsythe ID. 1995. Two voltage-dependent K+ conductances with complementary functions in postsynaptic integration at a central auditory synapse. *The Journal of Neuroscience* **15**:8011–8022 PMID: 8613738.,

Brooke RE, Moores TS, Morris NP, Parson SH, Deuchars J. 2004. Kv3 voltage-gated potassium channels regulate neurotransmitter release from mouse motor nerve terminals. *The European Journal of Neuroscience* **20**:3313–3321. DOI: https://doi.org/10.1111/j.1460-9568.2004.03730.x, PMID: 15610163

Brooke RE, Corns L, Edwards IJ, Deuchars J. 2010. Kv3.3 immunoreactivity in the vestibular nuclear complex of the rat with focus on the medial vestibular nucleus: Targeting of Kv3.3 neurones by terminals positive for vesicular glutamate transporter 1. *Brain Research* **1345**:45–58. DOI: https://doi.org/10.1016/j.brainres.2010.05.020

Cao XJ, Shatadal S, Oertel D. 2007. Voltage-sensitive conductances of bushy cells of the Mammalian ventral cochlear nucleus. *Journal of Neurophysiology* **97**:3961–3975. DOI: https://doi.org/10.1152/jn.00052.2007, PMID: 17428908

Chang SY, Zagha E, Kwon ES, Ozaita A, Bobik M, Martone ME, Ellisman MH, Heintz N, Rudy B. 2007. Distribution of Kv3.3 potassium channel subunits in distinct neuronal populations of mouse brain. *The Journal of Comparative Neurology* **502**:953–972. DOI: https://doi.org/10.1002/cne.21353, PMID: 17444489

Chen Z, Cooper B, Kalla S, Varoqueaux F, Young SM. 2013. The Munc13 proteins differentially regulate readily releasable pool dynamics and calcium-dependent recovery at a central synapse. *The Journal of Neuroscience* **33**:8336–8351. DOI: https://doi.org/10.1523/JNEUROSCI.5128-12.2013, PMID: 23658173

Choudhury N, Linley D, Richardson A, Anderson M, Robinson SW, Marra V, Ciampani V, Walter SM, Kopp-Scheinpflug C, Steinert JR, Forsythe ID. 2020. Kv3.1 and Kv3.3 subunits differentially contribute to Kv3 channels and action potential repolarization in principal neurons of the auditory brainstem. *The Journal of Physiology* **598**:2199–2222. DOI: https://doi.org/10.1113/JP279668

Coetzee WA, Amarillo Y, Chiu J, Chow A, Lau D, McCormack T, Moreno H, Nadal MS, Ozaita A, Pountney D, Saganich M, Vega-Saenz de Miera E, Rudy B. 1999. Molecular diversity of K+ channels. *Annals of the New York Academy of Sciences* **868**:233–285. DOI: https://doi.org/10.1111/j.1749-6632.1999.tb11293.x, PMID: 10414301

Cuttle MF, Rusznák Z, Wong AY, Owens S, Forsythe ID. 2001. Modulation of a presynaptic hyperpolarization-activated cationic current I(h) at an excitatory synaptic terminal in the rat auditory brainstem. *The Journal of Physiology* **534**:733–744. DOI: https://doi.org/10.1111/j.1469-7793.2001.00733.x, PMID: 11483704

Desai RR, Kronengold JJ, Mei JJ, Forman SAS, Kaczmarek LKL. 2008. Protein kinase C modulates inactivation of Kv3.3 channels. *The Journal of Biological Chemistry* **283**:22283–22294. DOI: https://doi.org/10.1074/jbc.M801663200, PMID: 18539595

Devaux J, Alcaraz G, Grinspan J, Bennett V, Joho R, Crest M, Scherer SS. 2003. Kv3.1b is a novel component of CNS nodes. *The Journal of Neuroscience* **23**:4509–4518. DOI: https://doi.org/10.1523/JNEUROSCI.23-11-04509.2003, PMID: 12805291

Dodson PD, Billups B, Rusznák Z, Szûcs G, Barker MC, Forsythe ID. 2003. Presynaptic rat Kv1.2 channels suppress synaptic terminal hyperexcitability following action potential invasion. *The Journal of Physiology* **550**:27–33. DOI: https://doi.org/10.1113/jphysiol.2003.046250, PMID: 12777451

Du J, Haak LL, Phillips-Tansey E, Russell JT, McBain CJ. 2000. Frequency-dependent regulation of rat hippocampal somato-dendritic excitability by the K+ channel subunit Kv2.1. *The Journal of Physiology* **522**:19–31. DOI: https://doi.org/10.1111/j.1469-7793.2000.t01-2-00019.xm, PMID: 10618149

Elezgarai I, Díez J, Puente N, Azkue JJ, Benítez R, Bilbao A, Knöpfel T, Doñate-Oliver F, Grandes P. 2003. Subcellular localization of the voltage-dependent potassium channel Kv3.1b in postnatal and adult rat medial nucleus of the trapezoid body. *Neuroscience* **118**:889–898. DOI: https://doi.org/10.1016/s0306-4522(03)00068-x, PMID: 12732235

Espinosa F, McMahon A, Chan E, Wang S, Ho CS, Heintz N, Joho RH. 2001. Alcohol hypersensitivity, increased locomotion, and spontaneous myoclonus in mice lacking the potassium channels Kv3.1 and Kv3.3. *The Journal of Neuroscience* **21**:6657–6665 PMID: 11517255.,

Espinosa F, Torres-Vega MA, Marks GA, Joho RH. 2008. Ablation of Kv3.1 and Kv3.3 potassium channels disrupts thalamocortical oscillations in vitro and in vivo. *The Journal of Neuroscience* **28**:5570–5581. DOI: https://doi.org/10.1523/JNEUROSCI.0747-08.2008, PMID: 18495891

Fernandez FR, Morales E, Rashid AJ, Dunn RJ, Turner RW. 2003. Inactivation of Kv3.3 potassium channels in heterologous expression systems. *The Journal of Biological Chemistry* **278**:40890–40898. DOI: https://doi.org/10.1074/jbc.M304235200, PMID: 12923191

Forsythe ID. 1994. Direct patch recording from identified presynaptic terminals mediating glutamatergic EPSCs in the rat CNS, in vitro. *The Journal of Physiology* **479**:381–387. DOI: https://doi.org/10.1113/jphysiol.1994.sp020303, PMID: 7837096

Forsythe ID, Tsujimoto T, Barnes-Davies M, Cuttle MF, Takahashi T. 1998. Inactivation of presynaptic calcium current contributes to synaptic depression at a fast central synapse. *Neuron* **20**:797–807. DOI: https://doi.org/10.1016/S0896-6273(00)81017-X

Geiger JR, Melcher T, Koh DS, Sakmann B, Seeburg PH, Jonas P, Monyer H. 1995. Relative abundance of subunit mRNAs determines gating and Ca^{2+} permeability of AMPA receptors in principal neurons and interneurons in rat CNS. *Neuron* **15**:193–204. DOI: https://doi.org/10.1016/0896-6273(95)90076-4, PMID: 7619522

Geiger JR, Jonas P. 2000. Dynamic control of presynaptic Ca$^{(2+)}$ inflow by fast-inactivating K$^{(+)}$ channels in hippocampal mossy fiber boutons. *Neuron* **28**:927–939. DOI: https://doi.org/10.1016/s0896-6273(00)00164-1, PMID: 11163277

Graham BP, Wong AYC, Forsythe ID. 2004. A multi-component model of depression at the calyx of Held. *Neurocomputing* **58–60**:449–454. DOI: https://doi.org/10.1016/j.neucom.2004.01.080

Grissmer S, Nguyen AN, Aiyar J, Hanson DC, Mather RJ, Gutman GA, Karmilowicz MJ, Auperin DD, Chandy KG. 1994. Pharmacological characterization of five cloned voltage-gated K$^+$ channels, types Kv1.1, 1.2, 1.3, 1.5, and 3.1, stably expressed in mammalian cell lines. *Molecular Pharmacology* **45**:1227–1234 PMID: 7517498.,

Hennig MH, Postlethwaite M, Forsythe ID, Graham BP. 2008. Interactions between multiple sources of short-term plasticity during evoked and spontaneous activity at the rat calyx of Held. *The Journal of Physiology* **586**:3129–3146. DOI: https://doi.org/10.1113/jphysiol.2008.152124

Hernández-Pineda R, Chow A, Amarillo Y, Moreno H, Saganich M, Vega-Saenz de Miera EC, Hernández-Cruz A, Rudy B. 1999. Kv3.1-Kv3.2 channels underlie a high-voltage-activating component of the delayed rectifier K$^+$ current in projecting neurons from the globus pallidus. *Journal of Neurophysiology* **82**:1512–1528. DOI: https://doi.org/10.1152/jn.1999.82.3.1512, PMID: 10482766

Hoshi T, Zagotta WN, Aldrich RW. 1990. Biophysical and molecular mechanisms of Shaker potassium channel inactivation. *Science (New York, N.Y.)* **250**:533–538. DOI: https://doi.org/10.1126/science.2122519, PMID: 2122519

Hu H, Roth FC, Vandael D, Jonas P. 2018. Complementary tuning of Na$^+$ and K$^+$ channel gating underlies fast and energy-efficient action potentials in GABAergic interneuron axons. *Neuron* **98**:156–165. DOI: https://doi.org/10.1016/j.neuron.2018.02.024, PMID: 29621485

Ingham NJ, Pearson S, Steel KP. 2011. Using the auditory brainstem response (ABR) to determine sensitivity of hearing in mutant mice. *Current Protocols in Mouse Biology* **1**:279–287. DOI: https://doi.org/10.1002/9780470942390.mo110059, PMID: 26069055

Iwasaki S, Momiyama A, Uchitel OD, Takahashi T. 2000. Developmental changes in calcium channel types mediating central synaptic transmission. *The Journal of Neuroscience* **20**:59–65 PMID: 10627581.,

Jalabi W, Kopp-Scheinpflug C, Allen PD, Schiavon E, DiGiacomo RR, Forsythe ID, Maricich SM. 2013. Sound localization ability and glycinergic innervation of the superior olivary complex persist after genetic deletion of the medial nucleus of the trapezoid body. *The Journal of Neuroscience* **33**:15044–15049. DOI: https://doi.org/10.1523/JNEUROSCI.2604-13.2013, PMID: 24048834

Johnston J, Forsythe ID, Kopp-Scheinpflug C. 2010. Going native: voltage-gated potassium channels controlling neuronal excitability. *The Journal of Physiology* **588**:3187–3200. DOI: https://doi.org/10.1113/jphysiol.2010.191973

Joho RH, Ho CS, Marks GA. 1999. Increased gamma- and decreased delta-oscillations in a mouse deficient for a potassium channel expressed in fast-spiking interneurons. *Journal of Neurophysiology* **82**:1855–1864. DOI: https://doi.org/10.1152/jn.1999.82.4.1855, PMID: 10515974

Joho RH, Street C, Matsushita S, Knöpfel T. 2006. Behavioral motor dysfunction in Kv3-type potassium channel-deficient mice. *Genes, Brain, and Behavior* **5**:472–482. DOI: https://doi.org/10.1111/j.1601-183X.2005.00184.x, PMID: 16923152

Joris PX, Trussell LO. 2018. The Calyx of Held: A Hypothesis on the need for reliable timing in an intensity-difference encoder. *Neuron* **100**:534–549. DOI: https://doi.org/10.1016/j.neuron.2018.10.026, PMID: 30408442

Kaczmarek LK, Zhang Y. 2017. Kv3 Channels: Enablers of rapid firing, neurotransmitter release, and neuronal endurance. *Physiological Reviews* **97**:1431–1468. DOI: https://doi.org/10.1152/physrev.00002.2017, PMID: 28904001

Karcz A, Hennig MH, Robbins CA, Tempel BL, Rübsamen R, Kopp-Scheinpflug C. 2011. Low-voltage activated Kv1.1 subunits are crucial for the processing of sound source location in the lateral superior olive in mice. *The Journal of Physiology* **589**:1143–1157. DOI: https://doi.org/10.1113/jphysiol.2010.203331, PMID: 21224222

Kim JH, Kushmerick C, von Gersdorff H. 2010. Presynaptic resurgent Na$^+$ currents sculpt the action potential waveform and increase firing reliability at a CNS nerve terminal. *The Journal of Neuroscience* **30**:15479–15490. DOI: https://doi.org/10.1523/JNEUROSCI.3982-10.2010, PMID: 21084604

Kim JH, Renden R, von Gersdorff H. 2013. Dysmyelination of auditory afferent axons increases the jitter of action potential timing during high-frequency firing. *The Journal of Neuroscience* **33**:9402–9407. DOI: https://doi.org/10.1523/JNEUROSCI.3389-12.2013, PMID: 23719808

Kim WB, Kang KW, Sharma K, Yi E. 2020. Distribution of Kv3 Subunits in Cochlear Afferent and Efferent Nerve Fibers Implies Distinct Role in Auditory Processing. *Experimental Neurobiology* **29**:344–355. DOI: https://doi.org/10.5607/en20043, PMID: 33154197

Kopp-Scheinpflug C, Lippe WR, Dörrscheidt GJ, Rübsamen R. 2003. The medial nucleus of the trapezoid body in the gerbil is more than a relay: comparison of pre- and postsynaptic activity. *Journal of the Association for Research in Otolaryngology* **4**:1–23. DOI: https://doi.org/10.1007/s10162-002-2010-5, PMID: 12098017

Kopp-Scheinpflug C, Tolnai S, Malmierca MS, Rübsamen R. 2008. The medial nucleus of the trapezoid body: comparative physiology. *Neuroscience* **154**:160–170. DOI: https://doi.org/10.1016/j.neuroscience.2008.01.088, PMID: 18436383

Kopp-Scheinpflug C, Pigott BM, Forsythe ID. 2015. Nitric oxide selectively suppresses IH currents mediated by HCN1-containing channels. *The Journal of Physiology* **593**:1685–1700. DOI: https://doi.org/10.1113/jphysiol.2014.282194, PMID: 25605440

Labro AJ, Priest MF, Lacroix JJ, Snyders DJ, Bezanilla F. 2015. Kv3.1 uses a timely resurgent K^+ current to secure action potential repolarization. *Nature Communications* **6**:10173. DOI: https://doi.org/10.1038/ncomms10173, PMID: 26673941

Leão RM, Kushmerick C, Pinaud R, Renden R, Li G-L, Taschenberger H, Spirou G, Levinson SR, von Gersdorff H. 2005. Presynaptic Na^+ channels: locus, development, and recovery from inactivation at a high-fidelity synapse. *The Journal of Neuroscience* **25**:3724–3738. DOI: https://doi.org/10.1523/JNEUROSCI.3983-04.2005, PMID: 15814803

Lewis AH, Raman IM. 2014. Resurgent current of voltage-gated Na^+ channels. *The Journal of Physiology* **592**:4825–4838. DOI: https://doi.org/10.1113/jphysiol.2014.277582, PMID: 25172941

Li M, Jan YN, Jan LY. 1992. Specification of subunit assembly by the hydrophilic amino-terminal domain of the Shaker potassium channel. *Science (New York, N.Y.)* **257**:1225–1230. DOI: https://doi.org/10.1126/science.1519059, PMID: 1519059

Li W, Kaczmarek LK, Perney TM. 2001. Localization of two high-threshold potassium channel subunits in the rat central auditory system. *The Journal of Comparative Neurology* **437**:196–218. DOI: https://doi.org/10.1002/cne.1279, PMID: 11494252

Lien CC, Jonas P. 2003. Kv3 potassium conductance is necessary and kinetically optimized for high-frequency action potential generation in hippocampal interneurons. *The Journal of Neuroscience* **23**:2058–2068 PMID: 12657664.,

Lipstein N, Chang S, Lin KH, López-Murcia FJ, Neher E, Taschenberger H, Brose N. 2021. Munc13-1 is a Ca^{2+}-phospholipid-dependent vesicle priming hub that shapes synaptic short-term plasticity and enables sustained neurotransmission. *Neuron* **109**:3980–4000. DOI: https://doi.org/10.1016/j.neuron.2021.09.054, PMID: 34706220

Lorteije JAM, Rusu SI, Kushmerick C, Borst JGG. 2009. Reliability and precision of the mouse calyx of Held synapse. *The Journal of Neuroscience* **29**:13770–13784. DOI: https://doi.org/10.1523/JNEUROSCI.3285-09.2009, PMID: 19889989

Lucas SJ, Michel CB, Marra V, Smalley JL, Hennig MH, Graham BP, Forsythe ID. 2018. Glucose and lactate as metabolic constraints on presynaptic transmission at an excitatory synapse. *The Journal of Physiology* **596**:1699–1721. DOI: https://doi.org/10.1113/JP275107, PMID: 29430661

Lujan B, Dagostin A, von Gersdorff H. 2019. Presynaptic diversity revealed by Ca^{2+}-permeable AMPA receptors at the calyx of Held synapse. *The Journal of Neuroscience* **39**:2981–2994. DOI: https://doi.org/10.1523/JNEUROSCI.2565-18.2019, PMID: 30679394

Macica CM, von Hehn C, Wang LY, Ho CS, Yokoyama S, Joho RH, Kaczmarek LK. 2003. Modulation of the Kv3.1b potassium channel isoform adjusts the fidelity of the firing pattern of auditory neurons. *The Journal of Neuroscience* **23**:1133–1141. DOI: https://doi.org/10.1523/JNEUROSCI.23-04-01133.2003

Meinrenken CJ, Borst JGG, Sakmann B. 2003. Local routes revisited: the space and time dependence of the Ca^{2+} signal for phasic transmitter release at the rat calyx of Held. *The Journal of Physiology* **547**:665–689. DOI: https://doi.org/10.1113/jphysiol.2002.032714, PMID: 12562955

Middlebrooks JC, Nick HS, Subramony SH, Advincula J, Rosales RL, Lee LV, Ashizawa T, Waters MF. 2013. Mutation in the kv3.3 voltage-gated potassium channel causing spinocerebellar ataxia 13 disrupts sound-localization mechanisms. *PLOS ONE* **8**:e76749. DOI: https://doi.org/10.1371/journal.pone.0076749, PMID: 24116147

Nakamura Y, Takahashi T. 2007. Developmental changes in potassium currents at the rat calyx of Held presynaptic terminal. *The Journal of Physiology* **581**:1101–1112. DOI: https://doi.org/10.1113/jphysiol.2007.128702, PMID: 17331991

Neher E, Sakaba T. 2008. Multiple roles of calcium ions in the regulation of neurotransmitter release. *Neuron* **59**:861–872. DOI: https://doi.org/10.1016/j.neuron.2008.08.019, PMID: 18817727

Neher E. 2017. Some subtle lessons from the calyx of Held synapse. *Biophysical Journal* **112**:215–223. DOI: https://doi.org/10.1016/j.bpj.2016.12.017, PMID: 28122210

Pan Z, Kao T, Horvath Z, Lemos J, Sul JY, Cranstoun SD, Bennett V, Scherer SS, Cooper EC. 2006. A common ankyrin-G-based mechanism retains KCNQ and NaV channels at electrically active domains of the axon. *The Journal of Neuroscience* **26**:2599–2613. DOI: https://doi.org/10.1523/JNEUROSCI.4314-05.2006, PMID: 16525039

Puente N, Mendizabal-Zubiaga J, Elezgarai I, Reguero L, Buceta I, Grandes P. 2010. Precise localization of the voltage-gated potassium channel subunits Kv3.1b and Kv3.3 revealed in the molecular layer of the rat cerebellar cortex by a pre-embedding immunogold method. *Histochemistry and Cell Biology* **134**:403–409. DOI: https://doi.org/10.1007/s00418-010-0742-6, PMID: 20857303

Ritzau-Jost A, Delvendahl I, Rings A, Byczkowicz N, Harada H, Shigemoto R, Hirrlinger J, Eilers J, Hallermann S. 2014. Ultrafast action potentials mediate kilohertz signaling at a central synapse. *Neuron* **84**:152–163. DOI: https://doi.org/10.1016/j.neuron.2014.08.036, PMID: 25220814

Ritzau-Jost A, Tsintsadze T, Krueger M, Ader J, Bechmann I, Eilers J, Barbour B, Smith SM, Hallermann S. 2021. Large, stable spikes exhibit differential droadening in excitatory and inhibitory neocortical boutons. *Cell Reports* **34**:108612. DOI: https://doi.org/10.1016/j.celrep.2020.108612, PMID: 33440142

Rowan MJM, Tranquil E, Christie JM. 2014. Distinct Kv channel subtypes contribute to differences in spike signaling properties in the axon initial segment and presynaptic boutons of cerebellar interneurons. *The*

Journal of Neuroscience **34**:6611–6623. DOI: https://doi.org/10.1523/JNEUROSCI.4208-13.2014, PMID: 24806686

Rowan MJM, DelCanto G, Yu JJ, Kamasawa N, Christie JM. 2016. Synapse-level determination of action potential duration by K^+ channel clustering in axons. *Neuron* **91**:370–383. DOI: https://doi.org/10.1016/j.neuron.2016.05.035, PMID: 27346528

Rudy B, Chow A, Lau D, Amarillo Y, Ozaita A, Saganich M, Moreno H, Nadal MS, Hernandez-Pineda R, Hernandez-Cruz A, Erisir A, Leonard C, Vega-Saenz de Miera E. 1999. Contributions of Kv3 channels to neuronal excitability. *Annals of the New York Academy of Sciences* **868**:304–343. DOI: https://doi.org/10.1111/j.1749-6632.1999.tb11295.x, PMID: 10414303

Rudy B, McBain CJ. 2001. Kv3 channels: voltage-gated K^+ channels designed for high-frequency repetitive firing. *Trends in Neurosciences* **24**:517–526. DOI: https://doi.org/10.1016/s0166-2236(00)01892-0, PMID: 11506885

Sakaba T, Neher E. 2003. Involvement of actin polymerization in vesicle recruitment at the calyx of Held synapse. *The Journal of Neuroscience* **23**:837–846. DOI: https://doi.org/10.1523/JNEUROSCI.23-03-00837.2003, PMID: 12574412

Schneggenburger R, Forsythe ID. 2006. The calyx of Held. *Cell and Tissue Research* **326**:311–337. DOI: https://doi.org/10.1007/s00441-006-0272-7, PMID: 16896951

Sierksma MC, Borst JGG. 2017. Resistance to action potential depression of a rat axon terminal in vivo. *PNAS* **114**:4249–4254. DOI: https://doi.org/10.1073/pnas.1619433114, PMID: 28373550

Sinclair JL, Fischl MJ, Alexandrova O, Heß M, Grothe B, Leibold C, Kopp-Scheinpflug C. 2017. Sound-Evoked Activity Influences Myelination of Brainstem Axons in the Trapezoid Body. *The Journal of Neuroscience* **37**:8239–8255. DOI: https://doi.org/10.1523/JNEUROSCI.3728-16.2017, PMID: 28760859

Song P, Yang Y, Barnes-Davies M, Bhattacharjee A, Hamann M, Forsythe ID, Oliver DL, Kaczmarek LK. 2005. Acoustic environment determines phosphorylation state of the Kv3.1 potassium channel in auditory neurons. *Nature Neuroscience* **8**:1335–1342. DOI: https://doi.org/10.1038/nn1533, PMID: 16136041

Southan AP, Robertson B. 2000. Electrophysiological characterization of voltage-gated K^+ currents in cerebellar basket and Purkinje cells: Kv1 and Kv3 channel subfamilies are present in basket cell nerve terminals. *The Journal of Neuroscience* **20**:114–122. DOI: https://doi.org/10.1523/JNEUROSCI.20-01-00114.2000

Steinert JR, Robinson SW, Tong H, Haustein MD, Kopp-Scheinpflug C, Forsythe ID. 2011. Nitric oxide is an activity-dependent regulator of target neuron intrinsic excitability. *Neuron* **71**:291–305. DOI: https://doi.org/10.1016/j.neuron.2011.05.037, PMID: 21791288

Stevens SR, Longley CM, Ogawa Y, Teliska LH, Arumanayagam AS, Nair S, Oses-Prieto JA, Burlingame AL, Cykowski MD, Xue M, Rasband MN. 2021. Ankyrin-R regulates fast-spiking interneuron excitability through perineuronal nets and Kv3.1b K^+ channels. *eLife* **10**:e66491. DOI: https://doi.org/10.7554/eLife.66491, PMID: 34180393

Stevens SR, van der Heijden ME, Ogawa Y, Lin T, Sillitoe RV, Rasband MN. 2022. Ankyrin-R Links Kv3.3 to the Spectrin Cytoskeleton and Is Required for Purkinje Neuron Survival. *The Journal of Neuroscience* **42**:2–15. DOI: https://doi.org/10.1523/JNEUROSCI.1132-21.2021, PMID: 34785580

Taschenberger H, von Gersdorff H. 2000. Fine-tuning an auditory synapse for speed and fidelity: developmental changes in presynaptic waveform, EPSC kinetics, and synaptic plasticity. *The Journal of Neuroscience* **20**:9162–9173. DOI: https://doi.org/10.1523/JNEUROSCI.20-24-09162.2000, PMID: 11124994

Taschenberger H, Leão RM, Rowland KC, Spirou GA, von Gersdorff H. 2002. Optimizing synaptic architecture and efficiency for high-frequency transmission. *Neuron* **36**:1127–1143. DOI: https://doi.org/10.1016/s0896-6273(02)01137-6, PMID: 12495627

Tatavarty V, Sun Q, Turrigiano GG. 2013. How to scale down postsynaptic strength. *The Journal of Neuroscience* **33**:13179–13189. DOI: https://doi.org/10.1523/JNEUROSCI.1676-13.2013, PMID: 23926271

Tollin DJ. 2003. The lateral superior olive: a functional role in sound source localization. *The Neuroscientist* **9**:127–143. DOI: https://doi.org/10.1177/1073858403252228, PMID: 12708617

Tolnai S, Englitz B, Scholbach J, Jost J, Rübsamen R. 2009. Spike transmission delay at the calyx of Held in vivo: rate dependence, phenomenological modeling, and relevance for sound localization. *Journal of Neurophysiology* **102**:1206–1217. DOI: https://doi.org/10.1152/jn.00275.2009, PMID: 19515955

Trimmer JS. 2015. Subcellular localization of K^+ channels in mammalian brain neurons: remarkable precision in the midst of extraordinary complexity. *Neuron* **85**:238–256. DOI: https://doi.org/10.1016/j.neuron.2014.12.042, PMID: 25611506

Tu LW, Deutsch C. 1999. Evidence for dimerization of dimers in K^+ channel assembly. *Biophysical Journal* **76**:2004–2017. DOI: https://doi.org/10.1016/S0006-3495(99)77358-3, PMID: 10096897

Wang LY, Gan L, Forsythe ID, Kaczmarek LK. 1998. Contribution of the Kv3.1 potassium channel to high-frequency firing in mouse auditory neurones. *The Journal of Physiology* **509**:183–194. DOI: https://doi.org/10.1111/j.1469-7793.1998.183bo.x, PMID: 9547392

Wang LY, Kaczmarek LK. 1998. High-frequency firing helps replenish the readily releasable pool of synaptic vesicles. *Nature* **394**:384–388. DOI: https://doi.org/10.1038/28645, PMID: 9690475

Weiser M, Vega-Saenz de Miera E, Kentros C, Moreno H, Franzen L, Hillman D, Baker H, Rudy B. 1994. Differential expression of Shaw-related K^+ channels in the rat central nervous system. *The Journal of Neuroscience* **14**:949–972 PMID: 8120636.,

Wong AYC, Graham BP, Billups B, Forsythe ID. 2003. Distinguishing between presynaptic and postsynaptic mechanisms of short-term depression during action potential trains. *The Journal of Neuroscience* **23**:4868–4877 PMID: 12832509.,

Wu XS, Subramanian S, Zhang Y, Shi B, Xia J, Li T, Guo X, El-Hassar L, Szigeti-Buck K, Henao-Mejia J, Flavell RA, Horvath TL, Jonas EA, Kaczmarek LK, Wu LG. 2021. Presynaptic Kv3 channels are required for fast and slow endocytosis of synaptic vesicles. *Neuron* **109**:938–946. DOI: https://doi.org/10.1016/j.neuron.2021.01.006, PMID: 33508244

Xu M, Cao R, Xiao R, Zhu MX, Gu C. 2007. The axon-dendrite targeting of Kv3 (Shaw) channels is determined by a targeting motif that associates with the T1 domain and ankyrin G. *The Journal of Neuroscience* **27**:14158–14170. DOI: https://doi.org/10.1523/JNEUROSCI.3675-07.2007, PMID: 18094255

Yang YM, Wang LY. 2006. Amplitude and kinetics of action potential-evoked Ca2+ current and its efficacy in triggering transmitter release at the developing calyx of Held synapse. *Journal of Neuroscience* **26**:5698–5708. DOI: https://doi.org/10.1523/JNEUROSCI.4889-05.2006, PMID: 16723526

Yang YM, Aitoubah J, Lauer AM, Nuriya M, Takamiya K, Jia Z, May BJ, Huganir RL, Wang LY. 2011. GluA4 is indispensable for driving fast neurotransmission across a high-fidelity central synapse. *The Journal of Physiology* **589**:4209–4227. DOI: https://doi.org/10.1113/jphysiol.2011.208066, PMID: 21690196

Yang YM, Wang W, Fedchyshyn MJ, Zhou Z, Ding J, Wang LY. 2014. Enhancing the fidelity of neurotransmission by activity-dependent facilitation of presynaptic potassium currents. *Nature Communications* **5**:4564. DOI: https://doi.org/10.1038/ncomms5564, PMID: 25078759

Yeung SYM, Thompson D, Wang Z, Fedida D, Robertson B. 2005. Modulation of Kv3 subfamily potassium currents by the sea anemone toxin BDS: significance for CNS and biophysical studies. *Journal of Neuroscience* **25**:8735–8745. DOI: https://doi.org/10.1523/JNEUROSCI.2119-05.2005, PMID: 16177043

Young SM, Veeraraghavan P. 2021. Presynaptic voltage-gated calcium channels in the auditory brainstem. *Molecular and Cellular Neurosciences* **112**:103609. DOI: https://doi.org/10.1016/j.mcn.2021.103609, PMID: 33662542

Zagha E, Manita S, Ross WN, Rudy B. 2010. Dendritic Kv3.3 potassium channels in cerebellar purkinje cells regulate generation and spatial dynamics of dendritic Ca2+ spikes. *Journal of Neurophysiology* **103**:3516–3525. DOI: https://doi.org/10.1152/jn.00982.2009, PMID: 20357073

Zhang Y, Zhang XF, Fleming MR, Amiri A, El-Hassar L, Surguchev AA, Hyland C, Jenkins DP, Desai R, Brown MR, Gazula VR, Waters MF, Large CH, Horvath TL, Navaratnam D, Vaccarino FM, Forscher P, Kaczmarek LK. 2016. Kv3.3 channels bind Hax-1 and Arp2/3 to assemble a stable local actin network that regulates channel gating. *Cell* **165**:434–448. DOI: https://doi.org/10.1016/j.cell.2016.02.009, PMID: 26997484

Zhang Y, Li D, Darwish Y, Fu X, Trussell LO, Huang H. 2022. KCNQ channels enable reliable presynaptic spiking and synaptic transmission at high frequency. *The Journal of Neuroscience* **42**:3305–3315. DOI: https://doi.org/10.1523/JNEUROSCI.0363-20.2022, PMID: 35256530